LO-173481

August 30, 2024 Docket No. 52-050

U.S. Nuclear Regulatory Commission
ATTN: Document Control Desk
One White Flint North
11555 Rockville Pike
Rockville, MD 20852-2738

SUBJECT: NuScale Power, LLC Submittal of “NuScale Power Module Short-Term Transient Analysis,” TR-121517, Revision 1

REFERENCE: 1. NuScale Power, LLC Submittal of the Technical Report, “NuScale Power Module Short-Term Transient Analysis,” TR-121517, Revision 0, dated December 31, 2022 (ML23001A018)

NuScale Power, LLC (NuScale) hereby submits Revision 1 of the “NuScale Power Module Short-Term Transient Analysis,” (TR-121517). This revision includes changes made during the Standard Design Approval Application audit. The next revision of the Standard Design Approval Application (Revision 2) will reference this revision of TR-121517.

Enclosure 1 contains the proprietary version of the report entitled, “NuScale Power Module Short-Term Transient Analysis,” TR-121517, Revision 1. NuScale requests that the proprietary version be withheld from public disclosure in accordance with the requirements of 10 CFR § 2.390. The enclosed affidavit (Enclosure 3) supports this request. Enclosure 1 has also been determined to contain Export Controlled Information. This information must be protected from disclosure per the requirement of 10 CFR § 810. Enclosure 2 contains the nonproprietary version of the report.

This letter makes no regulatory commitments and no revisions to any existing regulatory commitments.

If you have any questions, please contact Elisa Fairbanks at (541) 452-7872 or at efairbanks@nuscalepower.com.

I declare under penalty of perjury that the foregoing is true and correct. Executed on August 30, 2024.

Sincerely,

Carrie Fosaaen
Vice President, Regulatory Affairs
NuScale Power, LLC

Distribution: Mahmoud Jardaneh, Chief, New Reactor Licensing Branch, NRC
Getachew Tesfaye, Senior Project Manager, NRC
Prosanta Chowdhury, Senior Project Manager, NRC

Enclosure 1: “NuScale Power Module Short-Term Transient Analysis,” TR-121517-P, Revision 1, Proprietary Version
Enclosure 2: “NuScale Power Module Short-Term Transient Analysis,” TR-121517-NP, Revision 1, Nonproprietary Version
Enclosure 3: Affidavit of Carrie Fosaaen, AF-173482

Enclosure 1:

"NuScale Power Module Short-Term Transient Analysis," TR-121517-P, Revision 1, Proprietary Version

Enclosure 2:

"NuScale Power Module Short-Term Transient Analysis," TR-121517-NP, Revision 1, Nonproprietary Version

Licensing Technical Report

NuScale Power Module Short-Term Transient Analysis

August 2024

Revision 1

Docket: 52-050

NuScale Power, LLC
1100 NE Circle Blvd., Suite 200
Corvallis, Oregon 97330
www.nuscalepower.com

COPYRIGHT NOTICE

This report has been prepared by NuScale Power, LLC and bears a NuScale Power, LLC, copyright notice. No right to disclose, use, or copy any of the information in this report, other than by the U.S. Nuclear Regulatory Commission (NRC), is authorized without the express, written permission of NuScale Power, LLC.

The NRC is permitted to make the number of copies of the information contained in this report that is necessary for its internal use in connection with generic and plant-specific reviews and approvals, as well as the issuance, denial, amendment, transfer, renewal, modification, suspension, revocation, or violation of a license, permit, order, or regulation subject to the requirements of 10 CFR 2.390 regarding restrictions on public disclosure to the extent such information has been identified as proprietary by NuScale Power, LLC, copyright protection notwithstanding. Regarding nonproprietary versions of these reports, the NRC is permitted to make the number of copies necessary for public viewing in appropriate docket files in public document rooms in Washington, DC, and elsewhere as may be required by NRC regulations. Copies made by the NRC must include this copyright notice and contain the proprietary marking if the original was identified as proprietary.

Department of Energy Acknowledgement and Disclaimer

This material is based upon work supported by the Department of Energy under Award Number DE-NE0008928.

Table of Contents

Table of Contents

Table of Contents

List of Tables

List of Tables

List of Figures

List of Figures

List of Figures

List of Figures

Abstract

The Short-Term Transient Analysis technical report supplements information in the NuScale Power, LLC US460 standard design Final Safety Analysis Report relative to the dynamic analyses performed to evaluate structural response of the NuScale Power Module (NPM). Short-term transients are events caused by the failure or actuation of piping and valves, and include high-energy line breaks. These events result in system internal pressure waves and asymmetric cavity pressurization waves exterior to the pipe break or valve outlet.

Short-term transient events require special treatment due to the rapidly changing thermal hydraulic conditions and the resulting dynamic mechanical loads. In addition to the rapid nature of the transients, fluid-structure interactions are influential and require consideration.

This technical report provides an overview of the analytical methods used to simulate short-term transient mechanical loads, benchmarking performed to validate the analysis methods, and analysis results for selected short-term transient events for the NPM, as a representation of loads to be used as input to component analyses.

Executive Summary

This report identifies transients involving breaches in pressure boundaries inside and outside containment. Events that involve a breach in a high-energy pressure boundary require special treatment from a mechanical analysis standpoint due to the rapidly changing thermal hydraulic conditions and the resulting dynamic mechanical loads. In addition to the rapid nature of these transients, the fluid-structure interaction is modeled to ensure a bounding loading profile. For American Society of Mechanical Engineers Service Level B, C, and D events that include these dynamic mechanical loads, the stress analysis must confirm the structural design adequacy and ability, with no loss of safety function, of the reactor vessel internals and portions of the reactor coolant pressure boundary that are not compromised, to withstand the loads from breaches in high-energy pressure boundaries in combination with the safe shutdown earthquake as specified in the NuScale Power Module component design specifications.

Commercially available software applications can be used for transient analysis of complicated structures. NuScale reviewed recent industry experience with similar applications to develop its short-term transient analysis methodology. For consistency with other NuScale thermal hydraulic and mechanical applications, NuScale used the codes NRELAP5 and ANSYS for the dynamic analysis methodology. The thermal hydraulic code NRELAP5 is used to generate boundary conditions for the mechanical analysis, and ANSYS is used to simulate the fluid-structure interaction and calculate resultant time history loads. This approach is consistent with literature references.

Benchmarking is required for the dynamic models used to develop time histories applied as input to component stress analyses. The benchmarking results give confidence that the methodology provides acceptable simulation of the dynamic mechanical loads for the events identified. The benchmarking cases used for this analysis are integral and separate effects tests that provide experimental results of thermal hydraulic phenomena and the resulting mechanical loads. The results of the thermal hydraulic and mechanical dynamic analyses give a level of confidence that the dynamic loads associated with a short-term transient event are acceptably modeled for this design using the methodologies described. Benchmarking evaluation results are not sensitive to the thermal hydraulic boundary conditions, and an accurate structural response can be generated with known modeling simplifications. As summarized in Section 3.0, Validation Methods of the Short-Term Analysis Methodology, the parameters important to dynamic analysis compare favorably with experimental results. Based on the overall favorable agreement, application of a biasing margin on the thermal hydraulic or dynamic analysis results for the design is not necessary.

Structural loads that result from the high-energy breaches are specified as time history forces, moments, in-structure displacements and accelerations, and acoustic pressures. Resultant loads presented in this technical report contribute to the basis for the mechanical design of the NuScale Power Module.

1.0 Introduction

1.1 Purpose

This report documents the methodology for analyzing high-energy pressure boundary breaches due to the failure or actuation of piping and valves inside and outside containment. Breaches in the pressure boundary of high-energy systems require special treatment in mechanical design due to the large hydraulic forces that are rapidly generated during a depressurization event.

This report summarizes the high-energy breaches that are analyzed in the design and the planned analytical methods for simulating associated dynamic mechanical loads. The analytical methods are benchmarked using experimental results to ensure they are capable of accurately simulating the blowdown phenomena. This report provides quantitative comparisons of the performance of the short-term transient methodology with experimental high-energy line break (HELB) test data. The report demonstrates that the evaluation methodology is applicable to the high-energy breaches analyzed in the design, and provides an overview of the short-term transient analysis and results for representative cases.

1.2 Scope

The NuScale Power Module (NPM) design includes flow jet diffusers for reactor vent valves (RVVs) that discharge fluid into containment. Essential structures, systems, and components (SSC) are those required to shut down the reactor and mitigate the consequences of a postulated short term transient event. The purpose of jet diffusers, which are provided for the RVVs, is to prevent the valve discharge fluid jet from damaging nearby essential SSC.

As an engineering conservatism, the analysis did not credit the flow jet diffusers in the short-term transient methodology, benchmarking, or analysis. The reasons for this are as follows.

First, the system loads associated with the unconstrained postulated high energy breaches are low for the design, as shown in this report, and they do not need to be further reduced.

Second, the flow diffusers are designed to disrupt the effluent flow at the valve discharge outlets, compared to the unconstrained flow that is traditionally analyzed. This disruption reduces the acoustic energy, which minimizes the effects of the pressure wave propagating in containment. Similar to the internal pressure wave discussion, the system loads associated with asymmetric cavity pressure wave events are demonstrated to be low, so there is little benefit in benchmarking the performance of the flow diffusers to credit a further reduction in the loads associated with asymmetric cavity pressurization waves exterior to the valve outlet.

Thirdly, the short-term transient methodology relies on experimental data to benchmark the thermal hydraulic and mechanical analysis methods, to ensure that the simulation of the loads for postulated pipe breaks and valve actuations are sufficiently bounding. Significant research has been performed in the subject area of HELBs, and there are numerous experiments and standard problems available for benchmarking. However, there is not a significant body of research to benchmark the reduced flow conditions associated with the design's high-energy protective devices.

Also, the inadvertent actuation block feature of the reactor recirculation valve (RRV) prevents the valve from opening until the differential pressure between the reactor pressure vessel (RPV) and the containment vessel (CNV) decreases below a threshold that reduces the discharge mass flow rate and the accompanying blowdown loads. It is conservative for the analysis to ignore the inadvertent actuation block feature and model RRV blowdowns at the high differential pressure reactor coolant system (RCS) conditions.

Based on these considerations, the short-term transient methodology, benchmarking, and analysis conservatively neglect these protective devices.

1.3 Abbreviations

Table 1-1 Abbreviations

Term	Definition
ASME	American Society of Mechanical Engineers
BC	boundary condition
CNV	containment vessel
CRDM	control rod drive mechanism
CVCS	chemical and volume control system
DHRS	decay heat removal system
ECCS	emergency core cooling system
FW	feedwater
FSI	fluid-structure interaction
GDC	General Design Criteria
HDR	Heissdampf reactor
HELB	high-energy line break
JIT	jet impingement test
LOCA	loss-of-coolant accident
MS	main steam
NPM	NuScale Power Module
PSID	pounds per square inch differential
PWR	pressurized water reactor
PZR	pressurizer
RCPB	reactor coolant pressure boundary
RCS	reactor coolant system
RPV	reactor pressure vessel
RRV	reactor recirculation valve
RSV	reactor safety valve
RVI	reactor vessel internals
RVV	reactor vent valve

Table 1-1 Abbreviations (Continued)

Term	Definition
SG	steam generator
SSC	structures, systems, and components

Table 1-2 Definitions

Term	Definition
Acoustic pressure	The difference between the local pressure and equilibrium pressure due to a sound wave.
ANSYS	Engineering simulation software used for coupled FSI analysis.
Benchmarking	Analysis performed to demonstrate that the results of a simulation or hand calculation provide acceptable agreement with experimental results.
Blowdown load	A hydraulic load that develops as a result of the transient flow and pressure fluctuations following a valve actuation or a breach in a high-energy pressure boundary.
Essential boundary condition (BC)	BC in which a dependent variable, such as pressure or temperature, is applied to a domain boundary. Also called Dirichlet BC.
Essential SSC	Essential SSC are those required to shut down the reactor and mitigate the consequences of a postulated short term transient event.
Forcing function	An externally generated force that acts on a system, and is only a function of time.
Natural BC	BC in which a derivative of a dependent variable, such as pressure or temperature, is applied to a domain boundary. Also called Neumann BC.
NRELAP5	NuScale proprietary version of RELAP5-3D thermal hydraulic analysis code.
Pressurization load	A hydraulic load that develops as a result of a postulated high-energy pipe break or valve opening.
RELAP5-3D	Thermal hydraulic analysis code used for simulation of transients and postulated accidents in light water reactor systems.
Subcompartment	A fully or partially enclosed volume within the containment that houses or adjoins high-energy piping systems and restricts the flow of fluid to the main containment volume in the event of a postulated pipe rupture.
Terminal end	The extremities of a piping run that connect to structures, components (e.g., vessels, pumps, valves), or piping anchors that act as rigid constraints to piping motion and thermal expansion.

2.0 Background

Design requirements such as the American Society of Mechanical Engineers (ASME) Boiler Pressure Vessel Code (BPVC) ensures Seismic Category I components and supports are able to withstand design transients. Design transients define thermal-hydraulic conditions (i.e., pressure, temperature, and flow) for the NuScale Power Module. Bounding thermal-hydraulic design transients are defined for components of the reactor coolant pressure boundary. Short-term transients are events that are caused by the failure or actuation of piping and valves including high-energy line breaks. Such events result in internal pressure oscillations and external pressurization waves that are exterior to the pipe break or valve outlet.

This report discusses the methodology for analyzing high-energy reactor coolant pressure boundary breaches from piping and valves both inside and outside of containment. This short-term transient analysis is provided as a technical report to facilitate the submittal of proprietary and public information to the NuScale docket, in support of the NRC review of the technical information and results.

Flow jet diffusers are not credited in the short-term transient methodology, benchmarking, or analysis for this report. Justification for this decision is summarized in Section 1.2.

Additional background provided in subsequent sections includes a discussion of NuScale analysis methodology especially relevant to short-term transient events, regulatory requirements and guidance, and NuScale’s approach for regulatory compliance.

Bounding thermal-hydraulic design transients (Service Levels C and D) are defined for components of the reactor coolant pressure boundary. Short-term transients are events that are caused by the failure or actuation of piping and valves including high-energy line breaks. Such events result in internal pressure oscillations and external pressurization waves that are exterior to the pipe break or valve outlet.

2.1 Regulatory Requirements

Requirements for analyzing loads due to HELBs are from the General Design Criteria (GDC) of 10 CFR 50, Appendix A and the requirements for emergency core cooling modeling are found in 10 CFR 50, Appendix K. Applicable requirements that are implemented in the short-term transient methodology are provided below.

2.1.1 10 CFR 50 Appendix A, GDC 4

Compliance with GDC 4 is considered in the design of SSC to be protected from short term transient dynamic effects. Blowdown and asymmetric cavity pressurization are dynamic effects of a high energy valve actuation or pressure boundary breach that are the subject of this methodology.

2.1.2 10 CFR 50 Appendix A, GDC 14

Compliance with GDC 14 requires that the reactor coolant pressure boundary (RCPB) is designed to have a low probability of abnormal leakage, failure, or rupture.

Appropriate characterization and application of the blowdown and asymmetric cavity pressurization loads as design loads for affected SSC fulfills this requirement.

2.1.3 10 CFR 50 Appendix K, Section I.C.1

Compliance with this requirement is met by considering a spectrum of possible breaches in high-energy pressure boundaries. This spectrum includes instantaneous double-ended breaks in small piping inside the CNV and valve actuations.

For the purpose of characterizing blowdown and asymmetric cavity pressurization loads, the type of pipe break (circumferential or longitudinal) is not relevant. For the design, some valve actuations provide a greater flow area than is provided by postulated primary coolant pipe breaks.

2.1.4 10 CFR 50 Appendix K, Section I.C.1.b

To confirm the acceptability of the thermal hydraulic results, in addition to the benchmarking that is performed, the Moody model is used to confirm the thermal hydraulic results for postulated break locations and valve actuations.

2.1.5 10 CFR 50 Appendix K, Section I.C.1.d

In the thermal hydraulic model used for benchmarking, nodalization is chosen to provide agreement with the experimental results. Additionally, nodalization studies are performed to ensure that the nodalization is adequate and does not significantly affect the results.

2.1.6 10 CFR 50 Appendix K, Section I.C.2

Frictional losses and two-phase flow multipliers are investigated in the benchmarking and are chosen to provide good agreement with the experimental results. Based on the very short time period that is relevant for calculating the blowdown and asymmetric cavity pressurization loads, these inputs do not have a significant effect on the simulated results.

2.1.7 10 CFR 50 Appendix K, Section I.C.3

The thermal hydraulic analysis of high-energy line breaks and valve actuations must adequately characterize momentum changes, pressure losses and acceleration. These features are provided in the thermal hydraulic analysis code NRELAP5. Adequacy for the purpose of characterizing the high-energy pressure boundary breaches is demonstrated in the benchmarking analyses.

2.2 Regulatory Guidance

Guidance in the Standard Review Plan Sections 3.6.2, 3.9.2, and 3.9.5, and Branch Technical Position 3-4 are considered in the benchmarking methodology.

2.2.1 NUREG-0609, Asymmetric Blowdown Loads on Pressurized Water Reactor Primary Systems

NUREG-0609 (Reference 7.2.1) provides a historical and technical summary of blowdown load analysis for pressurized water reactors (PWRs), including criteria and guidance for conducting an evaluation.

NUREG-0609 Section 3.1.1 explains that although the effects of a sudden decompression of a PWR primary system can be determined by a straightforward calculation considering the loss-of-coolant accident (LOCA) pressure wave and its resulting interaction with internal structures of the reactor, the physical process is not as simple. The resulting motion of the core barrel to the decompression wave affects the local fluid pressure through the compressibility of the water; and the resulting hydrodynamic loads are typically reduced when this fluid-structure coupling is considered.

NUREG-0609 Section 3.1 identifies that the two steps required for calculating the hydraulic loads due to a blowdown are: (1) determine the transient pressure and velocity distribution throughout the system, using a thermal hydraulic code; and (2) convert the transient pressure and velocity data into equivalent transient forces through the primary system. The transient forces are then used as input, along with other LOCA loads, in the time-history structural analysis of the primary system. The procedure can be broken down into three categories: analytical development, application and system modeling, and computer-program verification.

Guidelines for developing loading functions for subcooled blowdown and cavity loads are summarized below.

Analytical Development:

- Use of homogeneous equilibrium is acceptable because during the modeling time of interest the system fluid is primarily subcooled. However, potential nonequilibrium effects should be considered. Note that for the spectrum of breaches that are analyzed in the design, not all system fluid is subcooled. Additionally, nonequilibrium effects are simulated using NRELAP5 and the degree of nonequilibrium is investigated as a part of the benchmarking analysis.
- The range of pressures and the sonic or acoustic wave speed should be described.
- The convergence criteria must ensure conservation of mass, momentum, and energy. These criteria are important if a one-dimensional code is used to model a multidimensional region.

- Essential BCs are the break opening time and area characteristics and must be justified.
- The discharge flow model for the postulated break is the system forcing function. As such, the treatment of the subcooled critical flow and potential nonequilibrium effects must be properly accounted for in the development of a discharge flow model.
- If fluid-structure coupling is considered, the method of incorporating the moving BC into the conservation equations must be justified.

Application and System Modeling:

- Use of homogeneous equilibrium is acceptable because during the modeling time of interest the system fluid is primarily subcooled. However, potential nonequilibrium effects should be considered.
- The ability of the model to track and transmit pressure waves must be demonstrated. At a minimum, a two-dimensional pressure field is required to adequately evaluate the effects of the decompression waves in an annulus region.
- The sensitivity of the model to spatial representation, time-step size, and to the various convergence criteria must be justified.

Computer Program Verification:

- The program and modeling procedure must be compared to selected problems and experimental data to demonstrate that the simulation provides good agreement with the phenomena.
- A comparison of the code performance with test data covering a wide range of system geometries is required. A Heissdampf reactor (HDR) test facility analysis is required as part of code verification. A partial list of additional acceptable experimental data is provided in Reference 7.2.9 through Reference 7.2.15.

Section 3.2 of Reference 7.2.1 discusses the analysis of asymmetric cavity pressurization loads. A subcompartment is defined as a fully or partially enclosed volume within the containment that houses or adjoins high-energy piping systems and restricts the flow of fluid to the main containment volume in the event of a postulated pipe rupture. Following a pipe rupture, a pressure wave develops within the cavity, generating loads on the components similar to those generated on the RVI. Reference 7.2.1 states the subcompartment pressure analyses are to be performed to determine asymmetric pressure loading on components and subcompartment walls, to ensure that the walls and component supports can withstand the forces and the reactor can be brought to a safe shutdown condition.

For the design, there are no subcompartments within the CNV. However, the containment itself is a small annular region in which a pressure wave could form and generate asymmetric loading on components inside the CNV. The loading on the components due to the pressure wave is bounded by other dynamic events, such as seismic and the blowdown transient, when the peak differential pressure across the vessel is reached.

Reference 7.2.1 states that codes like COMPARE and RELAP-4 MOD5 are typically used for subcompartment analyses. If other codes are used, confirmatory analysis is required. Additionally, Reference 7.2.1 provides guidelines for subcompartment nodalization and input assumptions that must be investigated via sensitivity studies.

2.3 Modeling Approaches from Literature

The following sections provide an overview of recent modeling approaches and a summary of their performance compared to the benchmark test data, where applicable.

2.3.1 R5FORCE

R5FORCE is a computer program developed by the Idaho National Laboratory that uses the output of RELAP5 to generate forcing functions for structural analysis. A description of the code and the user manual are documented in Reference 7.2.2. Using the hydrodynamic outputs of RELAP5, R5FORCE solves the force equation using the pressure and wall shear force terms. It is considered an improvement over legacy methods, which use pressure and fluid acceleration terms, because the use of the shear wall terms instead of the fluid acceleration terms eliminates numerical instabilities associated with computing the time derivative of the fluid acceleration term. The forcing functions generated by R5FORCE are intended for input into structural analysis codes, such as NUPIPE, SAP, or ADINA.

This code has not been used extensively in industry, and benchmarking results against experimental data are unknown. Based on advances in structural analysis codes, there does not appear to be an advantage in using an intermediate code to generate forcing functions. Modern structural analysis codes are capable of accepting thermal-hydraulic BCs and simulating FSI.

2.3.2 Computational Fluid Dynamics coupled with Finite Element Modeling

Reference 7.2.3 and Reference 7.2.8 use computational fluid dynamics coupled with finite element modeling codes to simulate the FSI and resulting structural responses. Both evaluations use pressure BCs from the two-phase system analysis code, APROS. In both evaluations, the pressure at a point in the nozzle exit without significant voiding is taken from the system analysis code and is applied as a BC in the computational fluid dynamics model. Reference 7.2.3 and Reference 7.2.8 show good agreement with the structural response of the core barrel region for the first 100ms. Both evaluations attribute the simulation errors after 100ms to the onset of two phase flow, which is not modeled with the computational fluid dynamics.

2.3.3 Acoustic-Structural Model with Pressure Boundary Condition

Another common analytical method is using an acoustic-structural model. Reference 7.2.3 provides an acoustic-structural model with a pressure BC from

APROS. Results are only in good agreement for 20 milliseconds (ms) following the transient initiation. Reference 7.2.3 attributes the deviations at larger times to the larger value of the dynamic pressure compared to the stagnation pressure. Dynamic pressure is not accounted for in the acoustic model because acoustic elements do not have a velocity.

2.3.4 Acoustic-Structural Model with Mass Flow Boundary Condition

Reference 7.2.4 improves on the acoustic-structural modeling approach by considering a different pipe break BC. Reference 7.2.4 uses a natural BC based on a mass flow rate from APROS. Results indicate good agreement with the experimental results beyond 100 ms.

2.3.5 Modeling Approach Selected for NuScale Analysis

The acoustic-structural modeling approach provides the highest accuracy and is the simplest analytical method of the literature approaches that have been investigated. The acoustic-structural modeling and BCs discussed in Reference 7.2.3 and Reference 7.2.4 are investigated for the NuScale design in Section 4.0.

2.4 NuScale Breach Sizes, Locations, and Exclusion Zones

2.4.1 Breach Sizes and Locations

The bounding piping breaks and other breaches of high-energy pressure boundaries that are included within the mechanical design-basis are identified in Table 2-1. An overview of the postulated breach locations with sizes is provided in Table 2-2. Further detail and justification are provided in Section 2.4.1.1 through Section 2.4.1.12.

As discussed in Section 1.2, the NPM design contains flow jet diffusers at the RVV discharge outlets. The purpose of jet diffusers is to prevent the valve discharge fluid jet from damaging nearby essential SSC. As a bounding engineering simplification, these protective components are not credited in the short-term transient methodology, benchmarking, or analysis and are omitted from discussion of the breach locations in the following sections.

Table 2-1 NuScale High-Energy Pressure Boundary Breaches

{{

}}2(a),(c),ECI

Table 2-2 High-Energy System Pipe or Valve with the Size for NPM-20 breach location identification

{{

}}2(a),(c),ECI

2.4.1.1 Spurious Opening of a Reactor Safety Valve

The reactor safety valves (RSVs) are located on top of the RPV and connect to the pressurizer steam space. They are designed primarily for steam service. Therefore, design basis blowdowns from this location are expected to be saturated.

Asymmetric cavity pressurization analysis is required to quantify the asymmetric loading generated due to the safety valve effluent entering containment during this event.

2.4.1.2 Spurious Reactor Vent Valve Actuation

The RVVs are located on top of the RPV and are designed for steam service.

It is recommended to include the minimum flow area along the valve exit path to model the choking point of the flow.

Asymmetric cavity pressurization analysis is required to quantify the asymmetric loading generated due to the RVV effluent entering containment during this event.

2.4.1.3 Spurious Reactor Recirculation Valve Actuation

The RRVs connect to the cold leg of the reactor coolant system (RCS) and the limiting spurious actuations are expected to be subcooled.

It is recommended to include the minimum flow area along the valve exit path to model the choking point of the flow.

Asymmetric cavity pressurization analysis is required to quantify the asymmetric loading generated based on RRV effluent entering containment during this event.

2.4.1.4 Chemical and Volume Control System Pipe Breaks

Chemical and volume control system (CVCS) pipe breaks are assumed to occur on piping carrying fluid between the CVCS and the RCS at locations inside the CNV. While breaks in this piping could also occur outside containment, the mass flow rates for breaks inside containment bound those outside containment due to additional friction and form losses.

There are five RCS piping connections to the RPV that could result in a small pipe break: the RPV high-point degasification line, the two pressurizer spray supply lines, the RCS injection line, and the RCS discharge line. These lines connect to the pressurizer steam space, the hot leg, and the cold leg and therefore represent saturated and subcooled blowdown conditions.

For analyzing blowdown loads, most of the design basis pipe break locations are bounded by the spurious RVV opening. The RVV flow area and venturi throat diameter are larger and located in the same regions as some of the piping connections; therefore, a break in one of the piping connections is expected to produce a similar but smaller dynamic response. The exception is the RCS injection line. Because this piping segment terminates in the riser, the structural response to the pressure wave internal to the riser after an injection line break should be modeled because this is a localized load for the RVI.

Asymmetric pressurization loads are expected to be similar to the loads generated during RVV and RRV opening, because the pipe breaks are postulated at the RPV shell and head nozzle welds.

2.4.1.5 Steam Generator Tube Failure

The steam generator (SG) is an American Society of Mechanical Engineers (ASME) Section III Class 1 component, and a mechanical failure leading to a full shear of a SG tube is considered credible for the design. However, the blowdown and asymmetric pressurization loads for a SG tube failure are bounded by loads generated with larger break sizes.

2.4.1.6 Steam Piping Failure

The steam piping inside containment is included in the containment penetration area and breaks are not postulated. The scope of this work is limited to piping up to the outermost containment isolation valve. There is no steam piping that is both outside the CNV and inside the outermost valve.

Because there are no breaks inside containment, asymmetric pressurization is not applicable for this location.

2.4.1.7 Feedwater Piping Failure

The feedwater piping inside containment is included in the containment penetration area and breaks are not postulated. The scope of this report is limited to the piping up to the outermost containment isolation valve. There is no feedwater piping that is both outside the CNV and inside the outermost valve.

Because there are no breaks inside containment, asymmetric pressurization is not applicable for this location.

2.4.1.8 Pressurizer Heater Port and Main Steam and Feedwater Access Ports

Class 1 and Class 2 penetrations that do not connect to high-energy lines do not require postulating a RCPB break.

2.4.1.9 Control Rod Assembly Ejection

A control rod ejection due to a rupture of the control rod drive mechanism (CRDM) housing is not considered a design basis mechanical failure in the NuScale design.

A gross failure of a CRDM housing is not considered a credible event because CRDM housings are ASME Section III Class 1 components, subject to hydrostatic testing to 125 percent of system design pressure in the shop and as a part of RPV hydrostatic testing. Housings are made of stainless steel with a high notch toughness value. Stress levels due to thermal transients are within the limits for ASME Section III Class 1 components, and pressure boundary welds meet the same design, procedure, examination, and inspection requirements as the welds on other ASME Section III Class 1 components.

2.4.1.10 Instrumentation & Control and Sensor Penetrations

A breach in the pressure boundary of an instrumentation and control cable penetration or a sensor nozzle is not identified as a design basis event. Class 1 penetrations that do not connect to high-energy lines do not require postulating an RCPB break.

2.4.1.11 Decay Heat Removal System

The decay heat removal system (DHRS) connects to the main steam (MS) piping outside of the CNV and upstream of the main steam isolation valves. The DHRS piping enters the reactor pool and connects to the DHRS condensers. A condensate return line is provided from the bottom of each DHRS condenser, through the CNV to a tee in the feedwater line inside containment.

Decay heat removal system piping outside containment is designed for break exclusion. The welds between the DHRS piping inside CNV and the CNV safe-end eliminate the need to postulate the break in the NPS 2 DHRS line inside the CNV which could impose the load on the SGS-MS and SGS-FW lines which are also in a break exclusion zone.

2.4.1.12 Containment Small Lines and Thermowells

A breach in the pressure boundary of a thermowell is not identified as a design basis event. Class 1 penetrations that do not connect to high-energy lines do not require postulating as an RCPB break.

Small lines are used for valve actuation and sensors. The maximum diameter of these lines is smaller than the RCS piping. The sensor taps are expected to connect to reducers, which are similar to or smaller than the diameter of the RCS piping; therefore, the blowdown and asymmetric cavity loads associated with breaks at these locations are considered bounded by the RCS piping.

2.5 Recommended Mechanical Design Transient Analysis Methodology

2.5.1 Blowdown Analysis

Based on the modeling methodologies identified in Section 2.3, Modeling Approaches from Literature, it is not necessary to use or develop a proprietary code to generate forcing functions for a dynamic mechanical analysis.

Consistent with Section 2.3.3 and Section 2.3.4, a modeling approach in which BCs are determined using a thermal hydraulic code and the FSI and dynamic mechanical response is analyzed in a multi-physics code is recommended. To provide consistency with other thermal hydraulic and mechanical applications, the codes NRELAP5 (Reference 7.2.19) and ANSYS (Reference 7.2.24) are used.

The blowdown loads due to breaches in high-energy systems are not expected to be limiting compared to other dynamic loads (such as seismic).

2.5.2 Asymmetric Cavity Pressurization Analysis

As discussed in Section 2.2.1, NUREG-0609, Asymmetric Blowdown Loads on PWR Primary Systems, the aspect of asymmetric cavity pressurization related to inducing loads on components, piping, and supports in the containment is relevant to the design. The phenomenon of asymmetric cavity pressurization is similar to the phenomenon internal to the vessel during the blowdown. The most significant difference is the thermal hydraulic properties through which the wave is transmitting. Asymmetric cavity pressurization inside containment results in slower wave transmission because of the lower speed of sound, and less FSI because of the lower density of the fluid.

2.6 Recommended Test Data for Benchmarking of Analysis Methodology

In accordance with Reference 7.2.1, benchmarking is required for the models used to develop the loadings for blowdown and asymmetric cavity pressurization analyses. Reference 7.2.1 requires the use of the HDR test data for benchmarking, and provides a list of other relevant test data that can be used for methodology benchmarking (described in Section 2.2.1).

A discussion of the test data recommended to benchmark the methodology is provided below.

2.6.1 Heissdampf Reactor Experiments

Per Reference 7.2.5, the purpose of the HDR test program was to provide experimental data for use in verification of physical models, numerical methods, and computer codes for the analysis of thermal hydraulic and structural coupling during the subcooled and saturated phases of a blowdown event. The HDR experiments consist of a series of break sizes and different degrees of subcooling in the downcomer, as described in Tables 3 and 9 of Reference 7.2.5. The reported experimental data consists of the thermal hydraulic and structural time history results; therefore, this experiment provides a means to benchmark both the ability for NRELAP5 to accurately simulate the short-term thermal hydraulic phenomena, as well as the ability for ANSYS to accurately simulate the structural response using either experimental data or NRELAP5 simulated results as BCs.

Table 2-3 compares key parameters in the HDR tests and Marviken test compared to the design. The HDR arrangement and test conditions are similar to the design, so this required benchmarking experiment is appropriate for the design. Figure 2-1 provides a visual comparison of the similarities between the NuScale and HRD test facility. The figure also shows the major components and postulated break locations for the design.

The HDR experiments were also performed to provide test data for asymmetric cavity pressurization events. The US-APWR used HDR V21.1 for benchmarking its subcompartment analysis code (Reference 7.2.7). Because the containment does not contain subcompartments, the benchmarking analysis is limited to the HDR results for the annular region surrounding the reactor vessel. Detailed modeling of the other HDR containment subcompartments is not necessary for methodology benchmarking.

Table 2-3 Heissdampf Reactor, Marviken, and NuScale Blowdown Comparison

Test Number	Pressure	Saturation Temp.	Upper Core Temp.	Downcomer Temp.	Downcomer Subcooling	Break Nozzle Length	Break Area
HDR V29.2(1)	90 bar	303.3°C	293°C	273°C	30°C	4.524 m	0.03142 m^2
HDR V31.1(1)	110 bar	318.1°C	308°C	268°C	50°C	1.369 m	
HDR V32				240°C	78°C		
Marviken JIT 11(2)	50 bar	263.9°C	262.4°C	262.4°C	saturated steam	27.5 m	0.07022 m^2
NPM-20 Operating Conditions	{{						

}}2(a),(c),ECI

Notes:

(1) Values for the HDR tests are taken from Tables 1, 3 and 9 in Reference 7.2.5.

(2) Values for the Marviken test are taken from Table 2-1 and Figure 2-2 of Reference 7.2.18, and Tables 2-2 and 2-5 in Reference 7.2.22.

Figure 2-1 Comparison of NuScale Power Module and Heissdampf Reactor

{{

}}2(a),(c),ECI

2.6.2 Marviken Experiments

The Marviken critical flow tests are similar to the HDR experiments, except the pressure vessel contains a steam space and some cases involve blowdown from the steam space. This test configuration is appropriate for benchmarking against the NuScale design because some breaches in the NuScale RCPB originate from the pressurizer steam space, such as actuation of the RVVs or some RCS line breaks. Use of this experiment for benchmarking demonstrates the ability of the NRELAP5 portion of the NuScale methodology to accurately simulate the short-term thermal hydraulic phenomena for breaks with little subcooling or at saturated conditions.

2.6.3 Bettis Hydraulic Pressure Pulse Experiment

The Bettis hydraulic pressure pulse experiment is a benchmarking case documented in Reference 7.2.6 and recommended for use in Reference 7.2.1. This experiment consists of a pressure pulse test conducted with two test sections: one solid and one flexible. A drop hammer and piston pulse was used to generate pressure pulses of up to 1150 psid over durations lasting between 6 to 47 milliseconds (ms). The fluid used in the experiments was room temperature water. The test series was performed with each test section at identical initial conditions to provide direct comparison of the increased FSI as a function of the test section rigidity.

This test configuration is appropriate for benchmarking against the NuScale design because it provides a good representation of the damping that can occur when a flexible member interacts with fluid; namely, to show that the structure absorbs the pressure wave energy and provides for reduced peak pressures. Use of this experiment for benchmarking demonstrates the ability of the ANSYS portion of the NuScale methodology to accurately simulate both low and high coupling between the fluid and the structure. A schematic of the test configuration is provided in Figure 4 of Reference 7.2.6.

3.0 Validation Methods of the Short-Term Analysis Methodology

The objective of the benchmarking analysis is to use NRELAP5 and ANSYS to simulate the thermal hydraulic conditions and resulting mechanical loads for various experimental configurations, and compare the simulation results to published literature testing data. The simulation results are compared to the experimental results in order to assess the error associated with the modeling methodology, and to identify important modeling parameters that must be specified to obtain appropriate results. Detailed objectives related to this benchmarking methodology that are addressed in this discussion are as follows:

- Define and justify a matrix of literature blowdown tests to be used for methodology benchmarking.
- Document the NRELAP5 and ANSYS models built to simulate the literature test configurations.
- Document the thermal and hydraulic BCs and mechanical load
- Compare simulated BCs and loads to experimental results and hand calculations, where applicable.
- Provide modeling guidelines for calculating the design basis loads from high-energy breaches. Identify which parameters have a significant effect on the results and how should they be treated to ensure this method provides appropriate loads.

A discussion of the validation process and applicable validation cases for NRELAP5 and ANSYS are provided in the following sections.

3.1 NuScale Design Basis, Important Loads, and Benchmarking Test Matrix

The benchmarking cases used for this analysis are integral and separate effects tests that provide experimental results of both the thermal hydraulic phenomena and the resulting mechanical loads. Research has been performed in the subject area of HELBs, and there are numerous experiments and standard problems that could be used for methodology benchmarking. Section 2.4.1, Breach Sizes and Locations, summarizes breach sizes, location, and phenomena that are important for the mechanical design basis events involving a breach in a high-energy system.

Table 2-1 and Table 2-2 summarize the specific mechanical loads of interest and associated breach location with size. The parameters of highest importance for methodology benchmarking are the simulated forces and displacements determined using ANSYS. The focus of this benchmarking is the mechanical loads resulting from blowdown and asymmetric cavity pressurization, which includes thrust forces at the break location.

Section 2.6 recommends three test configurations for methodology benchmarking; the Bettis hydraulic pressure pulse, HDR blowdown, and Marviken jet impingement tests (JITs). The basis and justification for selecting these three tests for benchmarking is provided in Section 2.6.

Table 3-1 shows how the selected experimental problems address the break locations and loads identified in Section 2.4.1 and comply with the guidance for dynamic analysis modeling provided in NUREG-0609 (Reference 7.2.1).

Section 3.2 provides a discussion of the HDR tests, a description of the NRELAP5 and ANSYS models used to simulate the experiments, and an overview of the sensitivity studies performed.

Section 3.3 provides a discussion of the Bettis hydraulic pressure pulse tests, and a description of the ANSYS models used to simulate the experiments.

Section 3.4 provides a discussion of the Marviken JIT, a description of the NRELAP5 models used to simulate the experiments, and an overview of the sensitivity studies performed.

Simulation analysis and results are discussed in Section 4.1 and Section 4.2.

Table 3-1 Phenomena and Parameters for Benchmarking

Mechanical Phenomena	Significant Benchmarking Parameters	Benchmarking Experiments	Justification
Blowdown	Mass flow rate Thrust force Fluid acceleration Static pressure Differential pressure Strain Displacement	HDR	The HDR experiments provide the means to compare the BCs and resulting RVI and RPV displacements and loads, for two break geometries and different initial thermal hydraulic conditions.
		Bettis	The Bettis hydraulic pressure pulse experiments are appropriate because they provide a means to compare displacements and forces resulting from a pressure pulse, with both high and low degrees of FSI.
		Marviken JIT	Marviken JIT provides stagnation initial conditions that are similar to the range of conditions experienced during a primary side break originating from the pressurizer steam region. The results of this experiment are applicable only to the NRELAP5 simulations.

Table 3-1 Phenomena and Parameters for Benchmarking (Continued)

Mechanical Phenomena	Significant Benchmarking Parameters	Benchmarking Experiments	Justification
Asymmetric cavity pressurization	Mass flow rate Thrust force Fluid acceleration Static Pressure Differential pressure Strain Displacement	HDR Bettis Marviken JIT	As discussed in Section 2.2.1, analysis is required to show that the NPM can withstand loads generated when a pressure wave develops in the annular space between the RPV and CNV. The primary difference between asymmetric cavity pressurization (outside the RPV) and blowdown (inside the RPV) in the design is the fluid properties. Because the density of the fluid in the containment is less than in the primary coolant, and the propagation of the pressure wave in containment is slower, the degree of interaction between the pressure wave and the CNV is less. Therefore, additional benchmarking cases to specifically assess this phenomenon for the CNV region are not required.

3.2 Heissdampf Reactor Experiments

The HDR test results are the preeminent reference related to blowdown loading analysis available, and are required to be used as a part of methodology benchmarking per NUREG-0609 (Reference 7.2.1). Table 2-3 provides a comparison of key parameters in the HDR tests, and Marviken compared to the NuScale design. This required benchmarking case is appropriate because the HDR arrangement and test conditions are similar to the design.

Reference 7.2.5 provides the experimental results of the first three blowdown tests performed with RVI at the HDR test facility. Per Reference 7.2.5, the purpose of the HDR test program was to provide experimental data for use in verification of physical models, numerical methods, and computer codes for the analysis of thermal hydraulic and structural coupling during the subcooled and saturated phases of a blowdown event. The HDR experiments consist of a series of break nozzle sizes and different degrees of subcooling in the downcomer, as described by Tables 3 and 9 of Reference 7.2.5.

The HDR experiments were also performed to provide test data for asymmetric cavity pressurization events. Because the NuScale containment is a single compartment, the phenomena of asymmetric cavity pressurization is limited to the annular region surrounding the RPV, and the annular region inside the reactor vessel is considered appropriate for benchmarking per Table 3-1.

The following tests are recommended for benchmarking: V29.2, V31.1, and V32. HDR testing case V34 is not included in this benchmark analysis because the key feature of this test was to simulate loose core barrel supports (snubbers), which is not applicable to the NuScale design. A comparison of the HDR cases is provided in Table 3-2. With the exception of V34, each degree of sub-cooling is represented in the tests recommended for benchmarking.

Table 3-2 Comparison of Heissdampf Reactor Test Conditions (Table 3 and 9 of Reference 7.2.5)

Test Number	Pressure (bar)	Upper Core Temperature (°C)	Downcomer Temperature (°C)	Downcomer Sub-cooling (°C)	Length of Break Nozzle (m)
V29.2	90	293	273	30	4.524
V31	110	308	268	50	1.369
V31.1 Note (1)					
V31.2 Note (2)					
V32 Note (3)			240	78	
V34		300	300	18	

Notes:

(1) Performed to demonstrate repeatability, lack of hysteresis effects, and general quality of measurements.
(2) Performed with additional instrumentation.
(3) GERMAN Standard Problem No. 5, Reference 7.2.4.

3.2.1 Heissdampf Reactor Experiments NRELAP5 Models

The NRELAP5 models for the HDR are comprised of fluid volumes and junctions. These components are used to represent the reactor vessel, discharge nozzle, break location, and containment.

An important factor in modeling the break location is ensuring that the model accurately predicts the subcooled blowdown and onset of choking at the break location. The NRELAP5 theory manual provides a detailed discussion of the models and correlations available in NRELAP5. The general modeling approach provided below is consistent with the example subcooled critical flow model.

The following sections detail the modeling geometries used to simulate the HDR experiments. Section 3.2.2 provides an overview of the variables investigated via sensitivity studies, and Section 3.2.2.4 discusses how the sensitivity studies are implemented in the model. A schematic of an example NRELAP5 model used to simulate the HDR experiments is provided in Figure 3-1. Different discharge nozzle nodalization and also component numbering conventions are used for the HDR V29.2, V31.1 and V32 simulations, and the HDR V31.1 sensitivity study.

Figure 3-1 NRELAP5 Models: Example Nodalization Schematic for Heissdampf Reactor Experiment

{{

}}$^{2(a),(c)}$

3.2.1.1 Reactor Vessel

The HDR reactor vessel is shown in Figure 3-2. The reactor vessel can either be modeled as a time dependent volume or a pipe. Time dependent volumes are typically used to model mass sources and sinks, and pressure BCs. Alternatively, the reactor vessel can be modeled as a pipe to simulate the BC using a finite mass and energy. Because of the short nature of these blowdown events, either component is appropriate to model the fluid in the RPV, as the fluid property changes in the RPV are small compared to the changes at the break location. The pipe component is selected for the benchmarking analyses. This RPV boundary condition is not a significant contributor to the results and a sensitivity study is not performed.

The HDR reactor vessel geometry is summarized in Table 3-3. Control option three is used to specify the reactor vessel fluid pressure and temperature, in accordance with the values from Table 3-2 for each transient case.

Figure 3-2 Schematic of the Heissdampf Reactor Pressure Vessel and Internals (Fig. 4-1 of Reference 7.2.16)

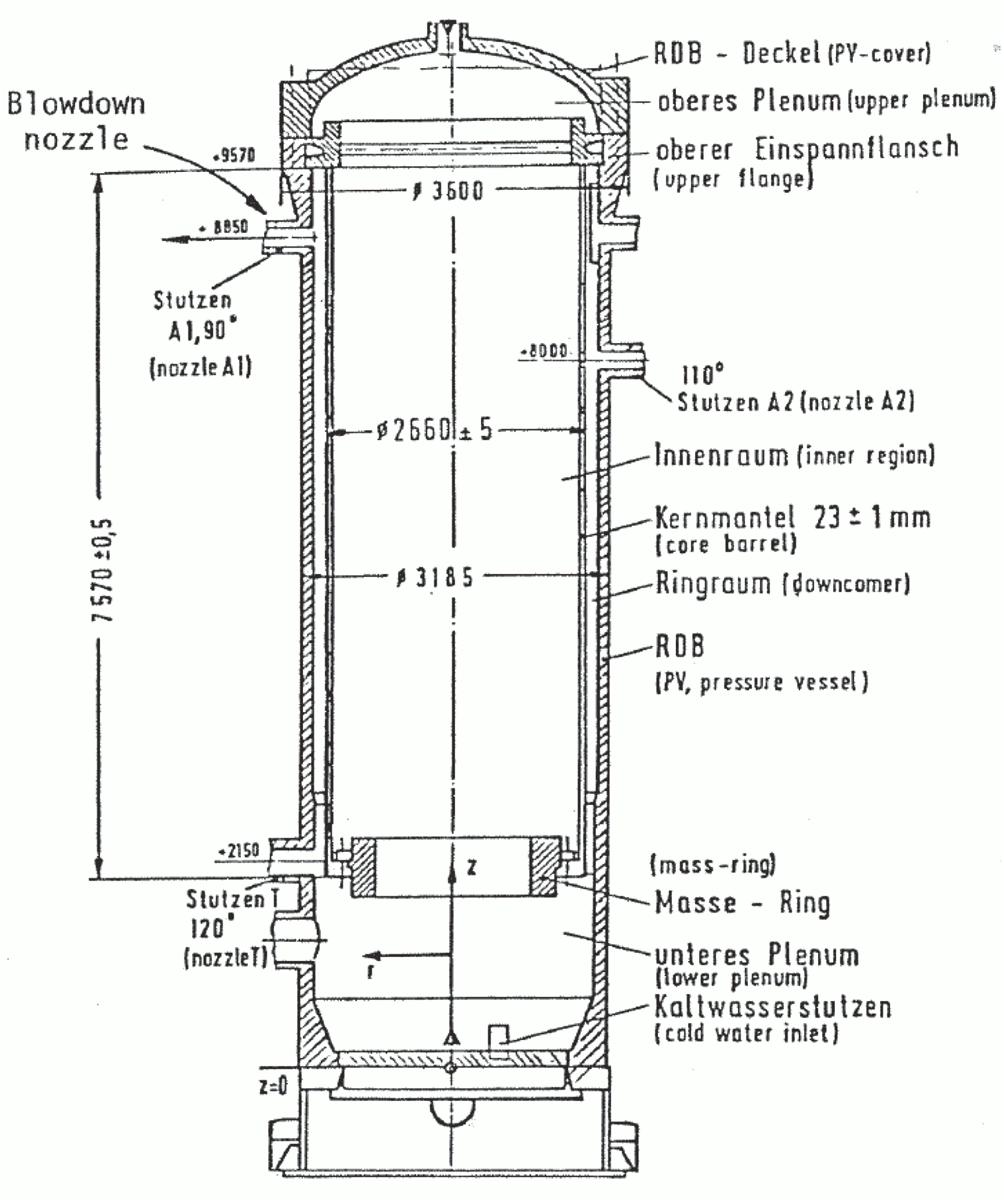

Table 3-3 Heissdampf Reactor Geometric Input Parameters

Parameter	Value		Reference
RPV outer diameter	10.45 ft	(3185 mm)$^{(1)}$	Figure 4-1 of Reference 7.2.16
Upper RPV thickness	4.41 in	(3184-2960)/2= 112mm)	Page 49, Enclosure 2-5 of Reference 7.2.23
Lower RPV thickness	5.59 in	(135mm+7mm= 142 mm)	Page 49, Enclosure 2-5 of Reference 7.2.23
Core barrel outer diameter	8.73 ft	(2660 mm)	Page 74, Enclosure 2-15 of Reference 7.2.23
Core barrel thickness	0.91 in	(23 mm)	Page 74, Enclosure 2-15 of Reference 7.2.23
Mass ring mass	14,881.2 lb	(6750 kg)	Page 4-9 of Reference 7.2.16
RPV height	35.47 ft	(10810 mm)	Page 49, Enclosure 2-5 of Reference 7.2.23
Core barrel length	24.84 ft	(7571 mm)	Page 74, Enclosure 2-15 of Reference 7.2.23
Break nozzle (A1) inside diameter	7.87 in	(200 mm)	Page 48, Enclosure 2-4 of Reference 7.2.23
Break nozzle length for V31.1 and V32	4.49 ft	(1369 mm)	Table 3 of Reference 7.2.5
Break nozzle length for V29.2	14.84 ft	(4524 mm)	Table 3 of Reference 7.2.5

Notes:

(1) The RPV outer diameter is specified as 3184 mm in certain references, such as pg. 49, enclosure 2-5 of Reference 7.2.23. The 1 mm difference does not have a detrimental effect on results.

3.2.1.2 Junction

A single junction component is used to connect the reactor vessel to the discharge nozzle. The model is simplified to include the downcomer as part of RPV vessel. Choking is disabled at this location to avoid erroneous oscillations between choking in the nozzle and at the break plane.

3.2.1.3 Discharge Nozzle

A pipe component is used to represent the piping segment leading up to the break location depicted in Figure 6 of Reference 7.2.5 along with the sensor locations. The cross sectional area is 0.03142 m^2 (0.338 ft^2), per the piping inner diameter specified. For case V29.2, the total length is 4.524 m (14.84 ft), and for the other cases a shorter pipe length of 1.3695 m (4.49 ft) is provided.

Choking is disabled in volumes and junctions within the nozzle, and smooth area changes are specified. Friction is modeled in the nozzle nodes with almost zero roughness value, considering a smooth surface finish ($5x10^{-6}$ ft) per Section 4.6.1 of Reference 7.2.17. The pressure and temperature initial conditions are specified in accordance with Table 3-2 for each transient case.

Sensitivity studies were performed to determine the optimal hydraulic nodalization as a function of the maximum time step. Section 3.2.2 contains additional discussion regarding the discharge nozzle nodalization.

3.2.1.4 Break Location

The break location is an important parameter that must be specified to accurately simulate the blowdown event. The three components that are suited for modeling a break location in NRELAP5 are junctions, trip valves, and motor valves. The difference between a trip and motor valve is that an opening rate can be specified for a motor valve, whereas the opening rate of the trip valve is instantaneous. The difference between using a junction and valve is that the time in the transient when the break opens can be specified, whereas if a junction is used to characterize a break it must open at a restart point. Reference 7.2.5 provides an estimate of the actual break opening times that were measured during the HDR experiments. A motor valve is selected for use to provide flexibility in simulating the time and rate of the break opening.

The ‘e’ flag is specified to be one at the break to activate the modified “PV” term in the energy equations. Full abrupt area change is specified at the break location. However, this selection does not affect the results because the downstream flow area in containment is large enough.

Three choking models in the NRELAP5 executable, Ransom-Trapp, Modified Henry-Fauske, and Moody are investigated in this evaluation. Sensitivity studies are performed to determine the optimal model and the most suitable model discharge coefficients during the blowdown events.

3.2.1.5 Containment

Use of a pipe to model the changing conditions in the containment is not necessary because downstream conditions are not relevant after the onset of choking, which occurs rapidly. The containment is specified as a time dependent volume at atmospheric pressure, with a static quality of one. The CNV is specified with the same length and area as the reactor vessel. This selection is arbitrary because the geometric properties of the containment have minimal effect on the fluid properties, and the fluid properties are irrelevant once choking occurs provided that containment pressure remains below the critical pressure.

3.2.2 Heissdampf Reactor Experiment Sensitivity Study Parameters

Sensitivity studies are performed to justify that an accurate match of the experimental data is found, and to quantify how a change in a modeling parameter affects the results. The parameters that are investigated in the sensitivity studies are the time step, spatial discretization, break opening time, and choking model type and coefficients. The following sections discuss the scope and implementation of the sensitivity studies. The sensitivity studies are performed using HDR V31.1, as this case represents the median amount of subcooling.

3.2.2.1 Time Step Control and Spatial Discretization

The considerations for the time step and acoustic Courant limit are discussed in Appendix A of the NuScale NRELAP5 input data requirement. The acoustic Courant limit is a function of the minimum node length and the speed of sound in the fluid, per Eq. 3-1:

$$\Delta t = \frac{\Delta x}{C_{water}} \qquad \text{Equation 3-1}$$

where,

Δt =maximum time step (s),

Δx =minimum node length in region of interest (ft), and

C_{water} =speed of sound in fluid (ft/s).

Table 3-4 provides a summary of the speed of sound, hydraulic nodalization, and the acoustic Courant limit for the V31.1 case. The 2, 4, 6 nodes are added to apply the NRELAP5 general guideline of pipe nodalization, L/D (nodal length over pipe inner diameter) is greater than 1.

A minimum time step of 10^{-11} seconds is specified in the input files. This value is not used in the analysis because the maximum time step remains lower than the material Courant limit; therefore, NRELAP does not perform a time step reduction during the transient. Note that a time step less than the material Courant limit is required to capture acoustic wave propagation in the nozzle upstream of the break location.

Table 3-4 Time Step as a Function of Node Length and Speed of Sound

{{

}}$^{2(a),(c),ECI}$

3.2.2.2 Break Opening Time

The use of prototypic break opening times versus the opening time of 0.001 seconds specified by NUREG-0609 is investigated to assess the effect on the NRELAP5 BCs. The sensitivity study is used to compare the experimental opening time to the NUREG-0609 recommended opening time, per Table 3-5. The break opening rate is determined by taking the reciprocal of the break opening time.

Table 3-5 Measured Break Opening Time (Table 4 of Reference 7.2.5)

{{

}}$^{2(a),(c),ECI}$

3.2.2.3 Choking Model Type and Coefficients

The three choking models available in the NRELAP5 executable used in this simulation are Ransom-Trapp, Modified Henry-Fauske, and Moody (Appendix A of NuScale NRELAP5 theory manual). The standard choking model in NRELAP5 is Ransom-Trapp. In this model, the subcooled, two phase and superheated coefficients can be specified. The default value for each coefficient is 1.0; lower values can be used for break locations that are more similar to orifices.

The default Henry-Fauske model discharge and thermal coefficients recommended in Section 6.3.2 of Reference 7.2.17 are 1.0 and 0.14, respectively. A discharge coefficient less than one provides for reduced flow from a break location. The NRELAP5 input data requirement uses a value of nearly 1.0 for break nozzles, although a value slightly less than 1.0 may be appropriate. A value of 0.8 is used as the median discharge coefficient for the sensitivity study. This value is chosen based on the values recommended in Appendix A of the NuScale NRELAP5 Input Data Requirements document.

The Moody model is required to calculate the discharging two phase fluid in composition by 10CFR 50 Appendix K as a conservatism. For the models, a range of values above and below (0.75 and 0.85) are investigated for the discharge coefficient, in order to investigate how the coefficient can be used to provide agreement with the experimental results.

Thermal non-equilibrium is not investigated for this sensitivity case, because the case is an example of a highly subcooled blowdown.

3.2.2.4 Heissdampf Reactor NRELAP5 Sensitivity Study Methodology

Table 3-6 provides a summary of the sensitivity parameters and ranges. The following section explains how the sensitivity studies are performed.

Table 3-6 Summary of Sensitivity Parameters for Heissdampf Reactor V31.1

{{

}}$^{2(a),(c),ECI}$

The HDR V31.1 test case is chosen for a full sensitivity analysis because literature results for pressure and mass flow rate BCs are available for this case, and because it is the average subcooling case compared to V29.2 and V32.

The three parameters that are expected to have the largest impact on accurately representing the pressure and mass flow rate near the break location are the choking model and coefficients, the nodalization of the discharge pipe, and the time step used for the simulation. This conclusion is based on Section 7.2 of Reference 7.2.19.

To minimize the number of required runs, the effect of the acoustic Courant limit (via the spatial discretization and time step) is investigated first in cases A1 through A6. Using the optimal result from the Case A sensitivity set, the choking model and discharge coefficients are investigated in cases B1 through B6. Using the optimal result from the Case B sensitivity set, the break opening time and model option sensitivities are investigated in cases C1 through C4. The methodology assumes that there are no synergistic effects between variables not investigated at the same time.

Mass flow rate, pressure, and density are used to calculate the fluid acceleration and thrust force BCs (Section 3.2.3.2 and Section 3.2.3.3). For each sensitivity case, the optimal results are determined based on which set of parameters provides the best agreement with experimental data. When a parameter could not be found to provide close agreement with both the experimental mass flow rate and experimental pressure, the parameter that provides better simulation of the mass flow rate was chosen. Out of the three parameters (pressure, mass flow rate and density), mass flow rate is important in order to accurately predict the fluid acceleration and thrust force because pressure is not used to determine fluid acceleration and the mass flow rate is squared in the thrust force equation.

A discussion of the sensitivity study results and the recommended simulation parameters are provided in Section 4.1.

3.2.3 ANSYS Modeling Methodology for Heissdampf Reactor Test Simulations

The dynamic loads associated with postulated piping breaks and valve discharges can be calculated by transient analysis using ANSYS. The HDR test cases V29.2, V31.1 and V32 are selected to perform the blowdown benchmark analysis. A half model with a symmetry BC is used, consistent with the HDR testing simulations in Reference 7.2.3 and Reference 7.2.4. The geometry, as shown in Figure 3-2, is symmetric except for several nozzles not in the symmetry plane (not modeled in ANSYS) and the bottom supports. The effect of these asymmetric details is not considered significant. Certain details of the HDR test vessel and blowdown nozzle geometry, such as the lower support skirt, are scaled from applicable references. The exact dimensions of geometric features for these regions of the test vessel do not have a significant effect on the simulation results; therefore, these simplifications are appropriate.

In the ANSYS models, the reactor vessel, core barrel and mass ring are represented by solid elements, and the fluid is represented by acoustic elements, which capture the coupling effect of the FSI at the fluid-structure interface. ANSYS provides various options for applying break BCs: (1) mass flow rate, (2) pressure, and (3) flow acceleration. As shown in Reference 7.2.3, because of the high flow velocity of water at the break location, the calculated pressure loads and structural responses caused by applying the acoustic pressure to acoustic elements at the break face, are clearly overpredicted after about 20 ms. Similar results are observed in this analysis as documented in Appendix D. In Reference 7.2.4, instead of an essential BC that applies acoustic pressure to the break face, the derivative of the mass flow rate is applied as a natural BC to the break face in ABAQUS, and good agreement with the measurements is obtained. In ANSYS, the equivalent BC is the flow acceleration for the acoustic elements. Therefore, the BC of flow acceleration is applied.

At the break location, the flow acceleration is applied to the fluid area and the thrust force is applied to the nozzle cross section area. The mass flow rates are used to calculate the flow acceleration at the postulated break locations. The mass flow rate and pressure are used to calculate the thrust force. An acoustic impedance BC is applied to the fluid area as the following:

```
CMSEL,S,BreakFace_Nodes

ESLN,S

SF,ALL,IMPD, ρ * V_c   !   Pa · s/m
```

Where ρ and V_c are water density and sonic speed.

3.2.3.1 Heissdampf Reactor ANSYS Models

The HDR test cases V29.2, V31.1, and V32 are modeled using ANSYS. These testing cases have the same geometry except that the length of the nozzle for V29.2 is 4524mm, but for V31.1 and V32 the nozzle length is only 1369 mm. The schematic of the HDR pressure vessel and internals is presented in Figure 4 of Reference 7.2.6. The selected testing cases are simulated in ANSYS transient analysis using the process discussed in Section 3.2.3.

As shown in Figure 3-3, the test model is simulated by three-dimensional (3D) structural elements in Figure 3-3(a) and acoustic elements in Figure 3-3(b), which capture the FSI effect at the interface. The model for the V31.1 and V32 (1.369 m discharge nozzle length) configuration is shown. The bottom of the foundation is fixed. The flow acceleration is applied to the break face of the fluid as discussed in Section 3.2.3.2, and the thrust force is applied to the nozzle as a pressure at the break location, as discussed in Section 3.2.3.3. The transient analysis is run for 0.1 second with a time step of 0.001 second. A sensitivity study is performed with a time step of 0.0001 second to ensure that the 0.001 second time step is sufficiently small to capture the acoustic wave frequency.

Figure 3-3 ANSYS Finite Element Analysis Model of the Heissdampf Reactor Pressure Vessel and Internals

{{

}}$^{2(a),(c)}$

3.2.3.2 Flow Acceleration at Break Locations

Using the mass flow rates from experiment data or NRELAP5, fluid acceleration can be calculated using the forward difference approximation of the derivative of the fluid velocity, which uses the time-dependent fluid density:

$$a_1(t) = \frac{1}{A_{break}}\left(\frac{\dot{m}(t)}{\rho(t)}\right)' \qquad \text{Equation 3-2}$$

where,

$a_1(t)$ = fluid acceleration (m/s^2),

$\dot{m}(t)$ = mass flow rate at the break (kg/s),

A_{break} =cross sectional area of break (m^2), and

$\rho(t)$ =density of the break effluent (kg/m^3).

Alternatively, the flow accelerations can be calculated by taking derivative of the mass flow rate. To avoid noisy behavior of the mass flow rate derivative curves, a smoothing is first performed using a high order polynomial curve fitting with a 0 intercept. The flow acceleration is then calculated by dividing the derivative of the polynomial curve by the break area and the average fluid density, as described by the following equation:

$$a_2(t) = \frac{f'(t)}{A_{break}\,\rho} \qquad \text{Equation 3-3}$$

where,

$a_2(t)$ = curve-fit fluid acceleration (m/s^2),

$f'(t)$ = derivative of best-fit mass flow rate curve (kg/s^2),

A_{break} = cross sectional area of break (m^2), and

ρ = average density of the break effluent (kg/m^3).

The two methods for calculating fluid acceleration are investigated using HDR V31.1 and HDR V32. The exact method, Eq. 3.2, is used for determining the fluid acceleration for HDR V32 (Appendix G). Eq. 3.3 is used for HDR V31.1, and provides good agreement with the experimentally determined fluid acceleration (Appendix F).

Figure 3-4 shows an example pipe break location (which is a portion of the ANSYS model provided in Figure 3-3). Solid elements that represent the pipe wall are shown as light grey nodes. In ANSYS, the acoustic elements representing the fluid inside the pipe are shown as dark grey nodes. Flow acceleration is applied as a body force to the acoustic element nodes on the break face. For example, the following code block reads acceleration data in the text file “acc.data” and applies to the break face “BreakFace_Nodes”, as shown in Figure 3-4.

Figure 3-4 ANSYS Nozzle End Nodes

{{

}}$^{2(a),(c)}$

```
*dim,ACC,TABLE,2360,,,TIME

*tread,ACC,acc,data    !Acceleration (m/s^2)

CMSEL,S,BreakFace_Nodes

BF,ALL,VELO,%ACC%,0,0

ALLS
```

3.2.3.3 Nozzle Wall Thrust Force at Break Locations

The thrust force generated by the fluid exiting the nozzle is equal to the thrust force exerted on the solid cross sectional area of the nozzle. The thrust force is calculated using Eq. 3.4, from page 86 of Reference 7.2.21. The mass flux is the mass flow rate per unit flow area, per Eq. 3.5. The total thrust of the fluid is equal in magnitude to the thrust on the nozzle, in accordance with Newton’s third law and as described by Eq. 3.6.

In ANSYS, the thrust force is applied to the nozzle wall cross-section area as an equivalent pressure, per Eq. 3.7. Note that because Eq. 3.4 uses the area and pressure at the break plane, the calculated thrust is applicable only to the break plane.

$$\frac{T_{fluid}}{A_{fluid}} = P_n - P_\infty + \frac{G^2 v_n}{g_c} \qquad \text{Equation 3-4}$$

$$G = \frac{\dot{m}}{A_{fluid}} \qquad \text{Equation 3-5}$$

$$T_{fluid} = T_{nozzle} = \left(P_n - P_\infty + \frac{G^2 v_n}{g_c}\right) A_{fluid} \qquad \text{Equation 3-6}$$

$$\frac{T_{fluid}}{A_{fluid}} = \left(P_n - P_\infty + \frac{G^2 v_n}{g_c}\right) \frac{A_{fluid}}{A_{nozzle}} \qquad \text{Equation 3-7}$$

where,

T_{fluid}/A_{fluid} = equivalent pressure, thrust per unit flow area (psi),

T_{nozzle}/A_{nozzle} = equivalent pressure, thrust per unit nozzle area (psi),

A_{nozzle} = cross-sectional metal area of break location (in.^{2}),

A_{fluid} = cross-sectional fluid flow area of break location (in.^{2}),

T_{nozzle} = thrust force on the metal area of break location (lb$_f$),

T_{fluid} = thrust force on the fluid flow area of break location (lb$_f$),

$\dot{m}$ = mass flow rate at the break (lb$_m$/s),

P_n = pressure at the nozzle discharge (psi),

P_∞ = pressure in the discharge reservoir (psi),

G = mass flux (lb$_m$/s-in.^{2}), and

υ_n = discharge specific volume (in^3/lb$_m$).

The thrust force is applied to the nozzle wall cross-section area nodes as an equivalent pressure data. For example, the following code block reads thrust pressure in the text file “ThrustPressure.data” and applies to the break face “Nozzle_End” nodes, as shown in Figure 3-4.

```
...

*dim,ThrustPressure,TABLE,52,,,TIME

*tread,ThrustPressure,ThrustPressure,data ! Thrust pressure(Pa)
SF,Nozzle_End,PRES,%ThrustPressure%

...
```

3.2.4 ANSYS Simulation Cases

For each of the HDR testing cases, three sets of pressure and mass flow rate time history results are obtained from the NRELAP5 simulations for the best estimate case, the lower bound flow and the upper bound flow. For HDR tests V31.1 and V32, the mass flow rates and pressures are also obtained from digitized experiment data. The fluid acceleration and thrust force BCs are calculated using three NRELAP5 sets of simulated pressure, mass flow rate, and density for experiments, except for HDR V29.2. For that experiment, the best-estimate fluid acceleration is applied for the three ANSYS validation cases. The two methods for calculating fluid acceleration (Equation 3-2 and Equation 3-3) are used for the HDR V31.1 and V32 validation cases, as identified in the second column of Table 3-7.

The ANSYS transient cases are summarized in Table 3-7. The flow acceleration and thrust force are calculated and provided to ANSYS model as inputs. They are also plotted in Appendix C.

For HDR tests V31.1 and V32, the acoustic pressure BC is also examined to confirm that the essential mass flow rate BC overestimates the dynamic response as shown in Reference 7.2.3. Because good agreement is not obtained for this BC, only the BCs from experimental data are applied, as BCs derived from NRELAP5 simulations would only introduce more error. The ANSYS transient cases for the acoustic pressure BC are summarized in Table 3-8.

Table 3-7 ANSYS Validation Matrix - Flow Acceleration Boundary Condition

{{

}}2(a),(c),ECI

Table 3-8 ANSYS Validation Matrix - Acoustic Pressure Boundary Condition

{{

}}2(a),(c),ECI

The dynamic responses produced by the ANSYS validation cases specified in Table 3-7 and Table 3-8 are compared to the experimental data or calculation data from available reports and published papers. The dynamic responses used to benchmark the ANSYS blowdown analysis methodology include absolute pressure and differential pressure in the fluid, and displacement and strain for the reactor vessel and core barrel.

Table 3-9 and Figure 3-5 summarize the dynamic responses that are used for benchmarking, the experimental sensor type and sensor location, and the figures in the appendices that compare the ANSYS transient analysis results with existing experimental and calculation data. Notes 2 - 5 of Table 3-9 document minor differences between the sensor locations reported in literature and the response location selected in the ANSYS simulation model. These minor deviations are less than 2 percent and are typically due to differences in the design versus as-built test facility dimensions.

Figure 3-5 ANSYS Finite Element Analysis Model Sensor Locations

{{

}}$^{2(a),(c)}$

Table 3-9 Dynamic Responses for Benchmarking

Response	Type	HDR	Location & Sensor (1)	Reference	Comparison Figure
1	Displacement	V29.2	Core barrel, KS1008 (1330, 90°, 8410)	Fig. 26 of Reference 7.2.5	Figure E-1
2	Displacement	V29.2	RPV, BS0106 (1590, 90°, 7350)	Fig. 28 of Reference 7.2.5	Figure E-2
3	Displacement	V29.2	RPV, BS0107 (1590, 180°, 7350)	Fig. 28 of Reference 7.2.5	Figure E-3
4	Displacement	V29.2	RPV, BS0108 (1590, 270°, 7350)	Fig. 28 of Reference 7.2.5	Figure E-4
5	Displacement	V31.1	RPV, BS0106 (1590, 90°, 7350)	Fig. 28 of Reference 7.2.5	Figure F-1
6	Displacement	V31.1	RPV, BS0107 (1590, 180°, 7350)	Fig. 28 of Reference 7.2.5	Figure F-2
7	Displacement	V31.1	RPV, BS0108 (1590, 270°, 7350)	Fig. 28 of Reference 7.2.5	Figure F-3
8	Pressure	V31.1	Fluid, BP9109 (1330, 90°, 8850)	Fig. 4-5 of Reference 7.2.16	Figure F-4
9	Pressure	V31.1	Fluid, BP9117 (1330, 270°, 8850)	Fig. 4-6 of Reference 7.2.16	Figure F-5
10	Pressure	V31.1	Fluid, BP9133 (1330, 88°, 5505) (2)	Fig. 4-7 of Reference 7.2.16	Figure F-6
11	Pressure	V31.1	Fluid, BP9140 (1330, 90°, 2300)	Fig. 4-8 of Reference 7.2.16	Figure F-7
12	Pressure	V31.1	Fluid, BP8301 (0, 0°, 10370)	Fig. 4-10 of Reference 7.2.16	Figure F-8
13	Diff. pressure	V31.1	Fluid, KP0009 (1307, 90°, 8850)	Fig. 4-12 of Reference 7.2.16	Figure F-9
14	Hoop strain	V31.1	Core barrel, KA2009 (1330, 90°, 8850) (3)	Fig. 4-15 of Reference 7.2.16	Figure F-10
15	Axial strain	V31.1	Core barrel, KA3008 (1330, 90°, 8850) (3)	Fig. 4-16 of Reference 7.2.16	Figure F-11
16	Displacement	V32	RPV, BS0106 (1590, 90°, 7350)	Fig. 8 of 1982 Schumann paper (Reference 7.2.20)	Figure G-1
17	Displacement	V32	RPV, BS0116 (1590, 90°, 5550)	Fig. A-47 of Reference 7.2.16	Figure G-2
18	Displacement	V32	Core barrel, KS1013 (1307, 90°, 7195)	Fig. A-112 of Reference 7.2.16	Figure G-3
19	Displacement	V32	Core barrel, KS1030 (1307, 90°, 2265) (4)	Fig. A-118 of Reference 7.2.16	Figure G-4
20	Displacement	V32	Core barrel, KS1032 (1307, 270°, 2265) (5)	Fig. A-120 of Reference 7.2.16	Figure G-5
21	Hoop strain	V32	Core barrel, KA2008 (1330, 90°, 8845) (3)	Fig. A-66 of Reference 7.2.16	Figure G-6
22	Axial strain	V32	Core barrel, KA3009 (1330, 90°, 8825) (3)	Fig. A-71 of Reference 7.2.16	Figure G-7

Table 3-9 Dynamic Responses for Benchmarking (Continued)

Response	Type	HDR	Location & Sensor (1)	Reference	Comparison Figure
23 (6)	Displacement	V32	Core barrel, KS1030 (1307, 90°, 2265) (4)	Fig. A-118 of Reference 7.2.16	Figure G-8
24 (6)	Displacement	V32	Core barrel, KS1032 (1307, 270°, 2265) (5)	Fig. A-120 of Reference 7.2.16	Figure G-9
25 (6)	Hoop strain	V32	Core barrel, KA2008 (1330, 90°, 8845) (3)	Fig. A-66 of Reference 7.2.16	Figure G-10
26 (6)	Axial strain	V32	Core barrel, KA3009 (1330, 90°, 8825) (3)	Fig. A-71 of Reference 7.2.16	Figure G-11

Notes:
(1) Cylindrical coordinate system (R, θ, Z) is used with R and Z in mm.
(2) Used (1330, 90°, 5505) for approximation in ANSYS.
(3) Used (1330, 90°, 8847) for approximation in ANSYS.
(4) Used (1307, 90°, 2300) for approximation in ANSYS.
(5) Used (1307, 270°, 2300) for approximation in ANSYS.
(6) Responses are presented for sensitivity study of time step.

3.3 Bettis Hydraulic Pressure Pulse Experiment

The Bettis hydraulic pressure pulse experiment was performed as part of the light water breeder reactor development program. The experiment is a separate effects benchmarking case documented in Reference 7.2.6. Reference 7.2.6 provides experimental results of flexible member tests that were performed to provide benchmarking of a computer code used to calculate pressure variations during a LOCA. This experiment is recommended for use in HELB benchmarking applications in Reference 7.2.1.

A schematic of the test configuration is provided in Figure 4 of Reference 7.2.6 and the test parameters defined in Table 3-10. The pressure pulse test apparatus consists of a pressure vessel with a piston on the top, and a test section that is mounted to the bottom of the vessel. This experiment consists of a pressure pulse test conducted with two different test sections: one solid and one flexible. A drop hammer and piston pulse were used to generate pressure pulses of up to 1150 psid over durations lasting between 6 to 47 ms. The fluid used in the experiments was room temperature water at 37.7 psia. The test series is performed with each test section at identical conditions to provide direct comparison of the increased FSI as a function of the test section rigidity. Cases 10 and 20 are selected for benchmarking because Reference 7.2.6 provides the most complete results for these particular cases. These cases provide a comparison of two different piston diameter sizes, with a flexible and solid wall.

Table 3-10 Bettis Hydraulic Pressure Pulse Test Parameters and Geometry (Table I of Reference 7.2.6)

Test Section Type	Run Number	Piston Diameter	Piston Weight	Drop Hammer Weight	Drop Height
Flexible wall	10F	1.0 inch	3.11 lb	42.3 lb	6.0 inch
	20F	2.0 inch	10.4 lb		
Rigid wall	10S	1.0 inch	3.11 lb		
	20S	2.0 inch	10.4 lb		

3.3.1 ANSYS Modeling Methodology for Bettis Hydraulic Pressure Pulse Test Simulations

The high pressure pulse for the Bettis hydraulic pressure pulse test can be simulated with a transient analysis in ANSYS. The test configuration as shown in Figure 4 of Reference 7.2.6 contains a cylindrical test vessel and a squared test section that can be represented by a 1/8th symmetric model. The vessel flange is not considered in the analysis models because the effect of this asymmetric detail is not significant for simulating the FSI, based on the best engineering practice. The piston, test vessel and test section are modeled using 3D structural elements and the water is modeled using 3D acoustic elements, as illustrated in Figure 3-6 for Run 10S/10F (with a 1-inch diameter piston).

A few parameters and BCs require calculation to define the model. These include the velocity of the piston just after impact, adjusted piston density (to account for the mass of the hammer), and the elastic modulus at the experimental pressure condition.

The initial velocity of the piston after the impact is calculated based on the momentum conservation principle with zero restitution. Because the hammer is not included in the ANSYS models, the density of the piston is adjusted to account for the mass of the hammer and the piston. The velocity of the piston after impact is applied as a BC for the transient mechanical analysis.

The velocity of the hammer, and adjusted density and velocity of the pistons are as follows:

$$t_{piston} = \sqrt{\frac{2h}{a_c}} \qquad \text{Equation 3-8}$$

$$v_{hammer} = a_c t_{piston} \qquad \text{Equation 3-9}$$

$$v_i = \frac{m_{hammer} v_{hammer}}{m_{hammer} + m_i} \qquad \text{Equation 3-10}$$

$$\rho_i = \frac{m_{hammer} + m_i}{V_i}$$ Equation 3-11

where,

t_{piston} = piston drop time to reach hammer (s),

h = drop height between piston and hammer (in.),

a_c = acceleration due to gravity (in./s^2),

v_i = velocity of the piston just after impact (in./s),

v_{hammer} = velocity of the hammer (in./s),

m_i = mass of the piston (lb),

m_{hammer} = mass of the hammer (lb),

V_i = volume of the piston (in,^{3}). and

ρ_i = adjusted density of the piston (lb/in.^{3}).

The solid test section in runs 10S and 20S is simulated by the same geometry as the flexible test section in runs 10F and 20F, but with a high elastic modulus. An elastic modulus of 1E10 psi is 1000 times higher than the flexible test section and no deflection is expected. Therefore, it is equivalent to that of a solid test section.

A piston damping coefficient that accounts for the friction between the piston and the sleeve is applied to the models based on the damping coefficients. The value is divided by eight because a 1/8th symmetric model is used. For Run 10S/10F, a total time of 30 ms is simulated, while for Run 20S/20F, a total time of 10 ms is simulated. A time step of 10^{-6} seconds is used as suggested on Page 15 of Reference 7.2.6. A stiffness damping constant of 5E-6 is used for the cases which provides a critical system damping ratio of about 1.5 percent for 1000 Hz. This use is deemed reasonable because the test results are recorded with a frequency response of about 900 Hz, as discussed on Page 3 of Reference 7.2.6.

The total absolute pressure is obtained by adding the acoustic pressure simulated by ANSYS at the top and bottom transducer locations and the static pressure which is 37.7 psia (Page 13 of Reference 7.2.6).

Figure 3-6 ANSYS Finite Element Analysis Model of Bettis Hydraulic Pressure Pulse Tests

{{

}}2(a),(c),ECI

Solid model components are shown on the left of Figure 3-6 and fluid elements are shown on the right of Figure 3-6. The acoustic elements are joined to the solid elements that represent the vessel and test section using a conformal mesh. Conformal mesh is recommended for FSI analysis to avoid convergence issues.

Because of the velocity boundary condition applied at the piston, the piston and acoustic body are joined using a bonded contact at the piston bottom surface.

3.4 Marviken Jet Impingement Test Experiment

The Marviken JITs were performed to assess the ability for NRELAP5 to match the required BCs when the initial fluid conditions upstream of the break location are saturated. This condition is applicable because the NuScale design has various high-energy lines and valves that contain steam. A summary of the testing initial conditions for JIT 1-12 are provided in Table 3-11.

Table 3-11 Comparison of Marviken test Conditions (Tables 2-2 and 2-4 of Reference 7.2.22)

Test Number	Nozzle Diameter (mm)	Pressure (MPa)	Sub-cooling (°C)	Water Level (m)	Discharge Entrance Level (m)
1	509	4.96	32	16.7	0.74
2	299	5.24	33	9.1	0.74
3	509	4.97	52	18.6	0.74
4	200	5.24	33	7.5	0.74
5	299	5.12	Less than 3	8.8	18.33
6	509	5.04	32	18.2	4.0
7	509	5.01	35	16.0	0.74
8	509	5.00	34	16.4	0.74
9	200	5.20	32	7.5	0.74
10	509	5.00	34	16.4	0.74
11	299	5.00	Less than 3	10.2	18.33
12	509	5.00	34	15.4	0.74

A schematic of the experimental setup is shown in Figure 3-7. A detailed discussion of the Marviken JITs and a portion of the testing results are provided in Reference 7.2.22. A detailed RELAP5-3D developmental assessment of Marviken JIT-11 is documented in Section 4.5 of Reference 7.2.18.

The cross-sectional area at the break location in the JITs is significantly larger than the piping and valves inside containment in the NuScale design, and the breaks modeled in the HDR test series. Therefore, this experiment bounds the thrust forces and fluid acceleration that could be experienced for breaks originating from saturated locations in the NuScale design.

Figure 3-7 Marviken Jet Impingement Test Schematic of Test Configuration (Figures 2-3 and 2-4 of Reference 7.2.22)

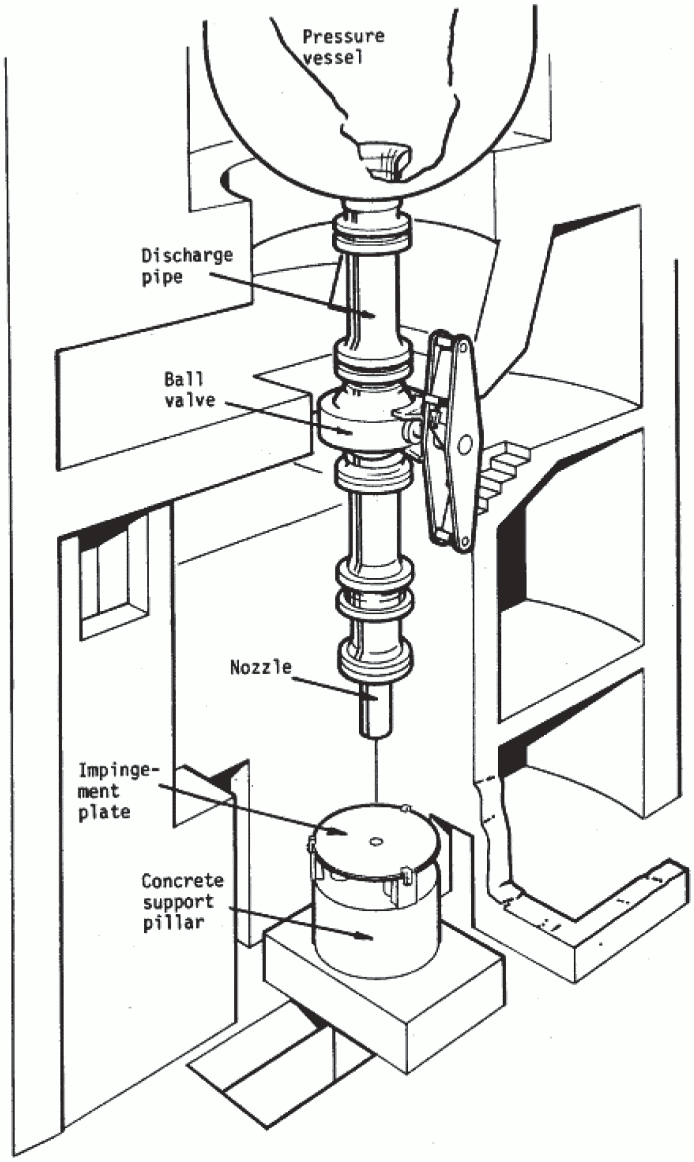

3.4.1 NRELAP5 Models-Marviken Jet Impingement

The NRELAP5 model for the Marviken JIT-11 experiment is comprised of fluid volumes and junctions representing and connecting the pressure vessel, discharge nozzle, break location, and containment, similar to the HDR simulation models. The following sections detail the modeling geometries used to simulate the Marviken JIT-11 experiment. An example NRELAP5 model schematic of the Marviken JIT experiment is provided in Figure 3-8.

Figure 3-8 NRELAP5 Models: Example Schematics for Marviken Experiment

{{

}}2(a),(c),ECI

3.4.1.1 Pressure Vessel and Standpipe

The pressure vessel BC is modeled as a pipe component, which allows NRELAP5 to calculate the change in fluid conditions in the reactor vessel over time. Because the JIT vessel contains saturated steam and liquid, the pipe is divided into nodes to specify a water level.

Modeling of the pressure vessel in this simulation is different than in Appendix A of Reference 7.2.18. Specifically, the JIT model in Reference 7.2.18 simulates the pressure vessel using a time dependent volume, and applies the experimentally-measured pressure time history to the volume. This is not judged to be an appropriate method for the purpose of this simulation because it is not possible to implement this simulation methodology for the plant break location (i.e., experimental data for the pressure time history in the reactor vessel for any NuScale break is and will not be available).

3.4.1.2 Discharge Pipe and Nozzle

The discharge pipe and nozzle characteristics are consistent with the modeling approach in Reference 7.2.22.

3.4.1.3 Break Plane

The break location is the most important parameter that must be specified to accurately simulate the blowdown event. A motor valve is selected for use to provide flexibility in simulating the time and rate of the break opening, consistent with the HDR simulations.

Consistent with the NuScale NRELAP5 input data requirement, the ‘e’ flag is specified and one at the break to activate the modified “PV” term in the energy equations. Full abrupt area change is specified at the break location. However, this selection does not affect the results because the downstream flow area in containment is so large.

3.4.1.4 Containment

Use of a pipe to model the changing conditions in the containment is not necessary because downstream conditions are not relevant after the onset of choking, which occurs rapidly in this event. Therefore, the containment is specified as a time dependent volume at atmospheric pressure, with a static quality of one. The CNV is specified with the same length and area as the reactor vessel. This selection is arbitrary because the geometric properties of the containment have minimal effect on the fluid properties, and the fluid properties are irrelevant once choking occurs provided that containment pressure remains below the critical pressure.

3.4.2 Jet Impingement Test Experiment Sensitivity Studies

Based on adequate agreement with experimental results using the optimal parameters identified via the HDR V31.1 sensitivity study, a sensitivity study for JIT 11 is not performed. Adequate agreement with the experimental data is obtained with the modeling parameters used for the HDR simulations.

4.0 Validation Analysis

4.1 Thermal Hydraulic Analyses

The time history results of the test cases are provided in Appendix A. Table 4-1 provides a summary of the simulation parameters that are used to achieve the benchmarking results for the HDR tests. The parameters summarized in Table 4-1 are determined using the sensitivity study for HDR V31.1 (per Section 3.2.2), and the results are discussed below. Experimental mass flow rates and pressures are plotted for sensor locations identified in Figure 6 of Reference 7.2.5. Select plots are provided in Appendix A and are discussed below.

Case A investigates time steps of 1 percent, 10 percent, and 100 percent of the acoustic Courant limit and spatial discretization of the discharge nozzle of 2, 4, or 6 nodes, and 16, 32, or 64 nodes (1 percent and 10 percent of the acoustic Courant limit only). Figure A-1 and Figure A-2 provide the sensitivity results for a time step of 10 percent of the acoustic Courant limit for three nodalization options (Case A2), and Figure A-3 and Figure A-4 provide results for the 1 percent acoustic Courant limit time step case (Case A5), Figure A-5 and Figure A-6 provide results for the 100 percent acoustic courant limit case (Case A8). Note that the node cases met the nodalization guide of (L/D > 1.0) do not match well with the testing data of the initial pressure drop. The pressure location at sensor RP3006 (Z=1369) is not exactly same location with NRELAP modeling results because the pressure in NRELAP is determined at the node center and different node size results in a different location at the last node. This difference is more prominent with larger node sizes for 2,4,6 nodes. Thus, plotting both RP3001 and RP3006 is helpful because it provides the spatial dependence of the pressure in the nozzle. The fine nodes match better with the testing data. The figures show that the degree of nodalization in the nozzle is more important for accurately matching the experimental pressure than for matching the mass flow rate, and that there is not a significant difference between a time step based on a 1 percent or 10 percent acoustic Courant limit. A nodalization of 32 or 64 nodes in the discharge nozzle provide equally acceptable results in the sensitivity study for HDR V31.1. A time step of 10 percent of the acoustic Courant limit is selected because a smaller time step does not improve simulation accuracy. This nodalization and time step are used as the basis for the set of Case B models.

Case B investigates three choking models and three discharge coefficients. As shown in Figure A-7 and Figure A-8, the Henry-Fauske choking model provides better agreement with the short-term pressure time history than the Ransom-Trap model. With manipulation of the choking model discharge coefficients, either model can provide good agreement with the mass flow rate experimental results, as shown in Figure A-9. For continuity, the Henry-Fauske model with a discharge coefficient of 0.8 provides good agreement with the mass flow rate results (Figure A-10), and is recommended. This choking model and discharge coefficient are used as the basis for the set of Case C models.

Case C investigates break opening time. As shown in Figure A-11 and Figure A-12, these parameters do not have a significant effect on the simulation results. Therefore, the NUREG-0609 recommended opening time is used for the HDR simulation models.

For the HDR simulations, Appendix C provides thrust force and fluid acceleration BCs using the experimental and NRELAP5 simulation data. Figure C-3 is calculated using Equation 3-3, and Figure C-5 is calculated using Equation 3-2. Figure C-3 uses the mass flow rate curve-fit and provides superior agreement with the experimental fluid acceleration BC. This is discussed further in Section 4.2.2.2 and Section 4.2.2.3.

The simulation parameters for the HDR sub-cooled tests and the Marviken saturated steam tests are provided in Table 4-1 and Table 4-2, respectively. Figure A-13 and Figure A-14 provide the NRELAP5 results for the HDR mass flow rate simulations. Figure A-15 through Figure A-17 provide the experimental and simulated density, mass flow rate, and thrust force for JIT-11 simulation. Good agreement is shown with the flow rate and density results. Differences in the simulated verses experimental forces are observed; however, these differences are within approximately 10 percent.

Table 4-1 Summary of Optimal Modeling Parameters for Heissdampf Reactor Benchmarking Cases

{{

}}$^{2(a),(c),ECI}$

As discussed in Section 3.4.2, the simulation parameters that showed good agreement for the HDR experiments also show good agreement for the JIT-11 simulation. The parameters used are summarized in Table 4-2.

From the NRELAP5 results, the mass flow rate is read from the valve that represents the break plane. Pressure and density are read from the last node in the discharge nozzle (i.e., directly upstream of the valve). For the HELB NRELAP5 simulations, the results are read from consistent locations to conform with the benchmarking results, unless additional sensitivity studies, benchmarking, or alternate calculations are used to justify an alternate method.

Table 4-2 Summary of Optimal Modeling Parameters for Marviken Met Impingement Test 11 Benchmarking Cases

{{

}}$^{2(a),(c),ECI}$

4.2 Mechanical Dynamic Analyses

4.2.1 Bettis Hydraulic Pressure Pulse Tests

The simulated pressures by ANSYS are compared with the measured pressures. Figure B-1 and Figure B-2 compare the simulated pressures at both top and bottom transducer locations for Run 10S and 10F, respectively, which show good agreement with the experimental data. Similarly, Figure B-3 and Figure B-4 compare the simulated pressures at both top and bottom transducer locations for Run 20S and 20F, respectively, which also show good agreement with the experimental data. The peak pressures are summarized below in Table 4-3. The data for experiment and FLASH-34 calculation results (Bettis reference analysis tool) are obtained from Table II of Reference 7.2.6. As shown in Table 4-3, the dynamic analysis in ANSYS is able to calculate the peak pressure reasonably accurately. The time-history pressure results in Appendix B also show good agreement.

Table 4-3 Summary of Peak Pressures (psia) for Bettis Hydraulic Pressure Pulse Test Simulations

Test Run		**10S**	**10F**	**20S**	**20F**
Top transducer (Figure 2-1)	Experiment data	1130	850	900	800
	FLASH-34	1190	950	1130	880
	ANSYS	{{			}}$^{2(a),(c),ECI}$
Bottom transducer (Figure 2-1)	Experiment data	1150	840	975	790
	FLASH-34	1260	935	1330	980
	ANSYS	{{			}}$^{2(a),(c),ECI}$

4.2.2 Heissdampf Reactor Results Overview

For HDR tests V29.2, V31.1 and V32, the fluid acceleration BC along with the thrust force results are presented in Appendix C.

Appendix D shows the structural model results with the pressure BC applied. The pressure between the nozzle and the core barrel decreases faster than that observed from experiments. This is expected because the ANSYS acoustic model is not able to capture the effect of high flow velocity of water at the break location when the acoustic pressure BC (i.e., the essential BC) is applied. The faster pressure decrease shown in Figure D-1 creates a higher differential pressure on the core barrel as shown in Figure D-2, which results in an overestimated structural response on the core barrel. Figure D-3 and Figure D-4 show that the radial displacements of the core barrel bottom at both the nozzle side and the opposite side are overestimated compared to the experimental data. Similar results have been presented in Figure 15 of Reference 7.2.3. Therefore, the acoustic pressure BC is not recommended for blowdown dynamic analysis.

Appendix E, Appendix F, and Appendix G present the comparison of dynamic responses for the two different flow acceleration BCs along with the thrust force, for HDR V29.2, V31.1 and V32, respectively. The depressurization propagation at 0.1 second is shown in Figure 4-1 for HDR V32. The core barrel deformations are presented at selected time points in Figure 4-2, which agree with the core barrel deformed shapes in Fig. 7 of Reference 7.2.4. The dynamic response comparisons are discussed in the following sections.

Figure 4-1 Heissdampf Reactor V32 Depressurization Propagation in Pa from the Break Location (at 100 ms)

{{

}}2(a),(c),ECI

Figure 4-2 Heissdampf Reactor V32 Core Barrel Deformations

{{

}}2(a),(c),ECI

4.2.2.1 Heissdampf Reactor V29.2

Appendix E provides the results for the HDR V29.2 simulations. The displacements on the core barrel and RPV are selected for comparison for this test case. The displacement of the core barrel relative to the RPV at the sensor location KS1008 is compared to the experimental data in Figure E-1, which shows reasonable agreement with the experiment data. The displacements of the RPV at the sensor location BS0106, BS0107 and BS0108 are compared with the experimental data in Figure E-2, Figure E-3, and Figure E-4, respectively. An overall good agreement has been achieved. It is also observed that the dynamic responses are not sensitive to the mass flow curves from the NRELAP5 model. The local discrepancy presented in these figures might be introduced from ANSYS modeling and simulation, digitizing of the data in Fig. 26 of Reference 7.2.5 (which is plotted for 1 second, not 0.1 seconds), and mass flow rate and pressure from the NRELAP5 prediction.

4.2.2.2 Heissdampf Reactor V31.1

The dynamic responses for HDR V31.1 are presented in Appendix F. For this set of simulations, the fluid acceleration calculated using the NRELAP5 result is determined using Eq. 3.3, which provides a smoothed fluid acceleration. Overall, these responses match the experimental data well. The displacements of the RPV at the sensor location BS0106, BS0107 and BS0108 are compared with the experimental data in Figure F-1, Figure F-2, and Figure F-3, respectively. The peak displacements for BS0106 and BS0108 are slightly overestimated. Considering that the RPV displacement is dependent on the RPV stiffness, the overestimation might be due to the model simplification that a symmetric model is used and the nozzle openings except for the break nozzle are not included in the ANSYS models. Overestimation of the displacement is conservative from the perspective of determining component dynamic loads; therefore, these results are acceptable. The simulated pressures are compared to the experimental data at the sensor locations in Figure F-4, Figure F-5, Figure F-6, Figure F-7, and Figure F-8, for BP9109, BP9117, BP9133, BP9140 and BP8301, respectively, which suggest that the propagation of the depressurization is slightly overpredicted. For example, at the end of 0.1 second, the pressure calculated for the experimental mass flow (denoted by green triangles in these figures) is about 0.5 MPa lower than the experimental data. This discrepancy could result from the assumed fluid element properties; however, the discrepancies are considered small and acceptable. It is also shown that the lower bound mass flow from NRELAP5 produces pressure match to the experimental data.

Figure F-9 compares the differential pressure at the core barrel inside and outside surfaces close to the break nozzle, which demonstrates agreement with the experimental data although the peak differential pressure is overestimated.

The hoop and axial strains of the core barrel outer diameter close to the break nozzle (sensors KA2009 and KA3008) are presented in Figure F-10 and Figure F-11, respectively, which demonstrate agreement with the experimental data. It is also shown that the ANSYS dynamic analysis produces a similar level of accuracy or better results compared to the WHAMSE code calculation reported in Reference 7.2.16.

4.2.2.3 Heissdampf Reactor V32

The dynamic responses for HDR V32 are presented in Appendix G. For this set of simulations, the fluid acceleration calculated using the NRELAP5 result is determined using Eq. 3.2, which provides an un-smoothed fluid acceleration. These responses match the experimental data reasonably well; however, the agreement is not as good using the smoothed fluid acceleration BC as was found for the HDR V31.1 simulations. The displacements of the RPV at the sensor location BS0106 and BS0116 are compared with the experimental data in Figure G-1 and Figure G-2, respectively. The local discrepancy might be due to the model simplification that a symmetric model is used, and the nozzle openings except for the break nozzle are not modeled in the ANSYS models.

The core barrel radial displacements relative to RPV are compared to the experimental data at the sensor locations KS1013, KS1030 and KS1032 in Figure G-3, Figure G-4, and Figure G-5, respectively. Larger discrepancies compared to the experimental data exist for the V32 simulations as compared to the V31.1 simulations. This difference is attributed to the use of an un-smoothed fluid acceleration BC.

The hoop and axial strains of the core barrel outer diameter close to the break nozzle (sensors KA2008 and KA3009) are presented in Figure G-6 and Figure G-7, respectively, which demonstrate good agreement with the experimental data.

As discussed in Section 3.2.3.1, the ANSYS transient analysis is run for 0.1 second with a time step of 0.001 second. A sensitivity study has been performed using the HDR V32 model with a time step of 0.0001 second to confirm that the 0.001 second time step is sufficient. As shown in Figure G-8 through Figure G-11, the results using the time step of 0.0001 second are only slightly different from the results using the time step of 0.001 second, which confirms that 0.001 second is a proper time step for use in the short-term transient analysis.

5.0 Validation Conclusions

The results of the thermal hydraulic and mechanical dynamic analyses documented in Section 4.0 provide a high level of confidence that the dynamic loads associated with a HELB can be acceptably modeled for the design using the methodologies described in Section 4.1. Section 4.2.2 shows that the dynamic analysis results are not sensitive to the thermal hydraulic BCs, and that a accurate structural response can be generated with known modeling simplifications. Therefore, a similar fidelity in the structural response can be obtained.

Appendix A through Appendix G demonstrate that the parameters important to dynamic analysis compare favorably with the experimental results. Therefore, uncertainty associated with the simulation methodology identified in Section 3.0 and the modeling simplification identified in Section 3.2-Section 3.4 are judged to be small.

Based on overall favorable agreement, in addition to the bounding simplification of neglecting the valve flow diffusers, application of a biasing margin on the thermal hydraulic or dynamic analysis results for the design is not necessary.

Section 5.1 provides the recommended NRELAP5 and ANSYS modeling guidelines to perform the HELB analyses consistent with the methodology and results of the benchmarking analyses for HDR Blowdown, Marviken Jet Impingement and Bettis Hydraulic Pressure Pulse.

5.1 NuScale Power Module Modeling Guidelines

5.1.1 NRELAP5 Modeling Guidelines

Hand calculations are performed to ensure the thermal hydraulic conditions calculated for the HELBs are reasonable. This hand calculation is an important step in modeling the HELBs because some breaks include extrapolation outside of the range of pressures, temperatures, and cross sectional areas over which benchmarking was performed. The hand calculations are performed using Figure 2.20(a) of Reference 7.2.21 and a steam table. The maximum mass flow rate is estimated based on the initial enthalpy and pressure of the fluid at the break location.

For blowdowns that are initially subcooled liquid or superheated steam, the mass flow rate at the time the system reaches saturation is also determined. At this time, the system pressure is roughly equal to the initial saturation pressure. The enthalpy is estimated by assuming the system has come to equilibrium at a saturated steam or saturated liquid condition. The energy contribution due to flow is not considered when specifying the stagnation pressure and enthalpy because the assumed pressure and temperature are relevant to the entire RCS, not only the break location.

Table 5-1 provides the modeling guidelines for simulating the thermal hydraulic BCs for the break locations. The modeling parameters are consistent with the discussion in Section 4.1. Engineering judgment is used in determining the acoustic Courant limit, the discharge coefficients, and a guideline of L/D. However, as described in

Section 4.2.2, the variations in structural response using the natural BC derived primarily from the curve-fit mass flow rate time history results are not significant.

For completeness, sensitivity studies are recommended to confirm that the BCs determined in the analysis, using the recommended acoustic Courant limit and discharge coefficients, are acceptable. The sensitivity ranges are provided in Table 5-1.

Because pressure, mass flow rate, and density time histories are necessary for generating the ANSYS BCs, the time step and plot frequencies must be specified such that for each case the plot frequencies are the same. Providing a common plot frequency for each event simplifies the data handling associated with calculating the ANSYS BCs.

Table 5-1 Recommended Modeling Parameters for the NuScale Break Locations

{{

}}$^{2(a),(c),ECI}$

5.1.2 ANSYS Modeling Guidelines

The structural responses to the blowdown event are simulated using ANSYS FSI transient analysis with the recommended BC, which is the flow acceleration corresponding to the derivative of the mass flow rate along with the thrust force at the break location. The acoustic pressure BC is not used because it is not able to capture the effect of the high flow velocity of water at the break location. The flow acceleration at the break location is calculated from the NRELAP5 mass flow rate. A high-order polynomial curve fitting is used to smooth the mass flow rate data to avoid any noisy behavior of the mass flow rate derivative curves, based on the results in Section 4.2.2.2 and Section 4.2.2.3. A uniform temperature and initial pressure may be assumed for the acoustic body. The flow acceleration and thrust force are calculated based on the constant density of the acoustic body.

A conformal mesh between the structure and the fluid is used for the modeling to avoid potential convergence issues with dissimilar meshes and contact definitions. The overall geometry and loading conditions should be reviewed to determine whether a half model can be used. The ability to use a half model is dependent on the break location and whether the expected deformation has symmetry planes. For general purpose models, a full model is needed.

A time step of 0.001 second is recommended for the short-term blowdown transient analysis based on the results of sensitivity studies (Section 4.2.2.3). The speed of sound associated with the acoustic elements used in this benchmarking analysis is greater than the average speed of sound throughout the fluid for the design. The time step of 0.001 seconds provides adequate resolution for tracking the pressure wave in the acoustic elements for the simulations.

If BCs other than thrust force and fluid acceleration are desired for dynamic analysis, sensitivity studies in ANSYS are performed to demonstrate that the BCs used are appropriate.

5.1.3 Discussion of Extrapolation

As identified in Table 5-2, the HDR and Marviken experiments provide similar break locations that are applicable to the NuScale design. However, not all parameters important for characterizing a break in the NuScale design are within the range of the parameters in the HDR and Marviken experiments. The parameters judged to be most important for accurately characterizing the break location are pressure, temperature, degree of subcooling, break area, and nozzle length.

The thermal hydraulic initial conditions are important because they determine the time at which choking at the break plane occurs. Once choking has occurred, the velocity of the flow is equal to the local speed of sound, and further decompression disturbances cannot propagate upstream. The break area is important because the smaller the break area, the faster choking occurs. The nozzle length is important in that it contributes to the degree of homogeneous equilibrium in the discharge fluid. A larger subcooling increases the magnitude of the decompression wave and the loads on internals. The estimated subcooling temperatures in the NPM design (during normal operating conditions) are higher by 9 deg C to 57 deg C than those of the HDR experiments, V32, V31.1 and V29, respectively. The density difference between NPM and HDR V29.2 is about 5 percent and this extrapolation to NPM conditions is less significant than the larger area in the HDR.

The normal operating downcomer temperature is not within the range of the Marviken and HDR experiments. The pressure and hot leg temperature exceed the conditions modeled in Marviken and HDR; however, the break areas in the design are smaller than HDR and Marviken. Therefore, despite the higher energy of the break locations, the critical mass flow rates are expected to be lower than the flow rates observed in the HDR and Marviken experiments.

Based on this discussion, it is not expected that significant extrapolation errors are present due to the differences between the benchmarking tests and the postulated break modeling. Further, any errors that may be present are bounded by the simplification of not modeling flow diffusers, which would reduce the dynamic loads associated with blowdown and asymmetric cavity pressurization.

Table 5-2 Heissdampf Reactor, Marviken, and NuScale High-Energy Line Break Comparison

Test Number	Pressure	Saturation Temperature	Upper Core Temp.	Downcomer Temp.	Downcomer Sub-cooling	Break Nozzle Length	Break Area
HDR V29.2(1)	90 bar	303.3°C	293°C	273°C	30°C	4.524 m	0.03142m^2
HDR V31.1(1)	110 bar	318.1°C	308°C	268°C	50°C	1.369 m	
HDR V32				240°C	78°C		
Marviken JIT 11(2)	50 bar	263.9°C	262.4°C	262.4°C	saturated steam	27.5 m	0.07022m^2
NPM-20 Operating Conditions	{{						}}$^{2(a),(c),ECI}$

Notes:

(1) Values for the HDR tests are taken from Table 3-2 or Tables 1, 3 and 9 in Reference 7.2.5.

(2) Values for the Marviken tests taken from Table 3-11 or from Table 2-1 and Figure 2-2 of Reference 7.2.18, and Tables 2-4 and 2-5 in Reference 7.2.22.

6.0 NuScale Power Module Asymmetric Cavity Pressurization and Blowdown

This section summarizes how the dynamic loads associated with the blowdown inside the RPV and asymmetric pressurization of the cavity between the CNV and the RPV are generated.

6.1 NRELAP5 Boundary Conditions for Asymmetric Cavity Pressurization and Blowdown

NRELAP5 analysis is performed to characterize the breaches in high energy lines and generate appropriate BCs for dynamic analysis. The break locations are analyzed in two groups:

- Subcooled primary coolant breaks
- Saturated primary coolant breaks

6.1.1 NRELAP5 Subcooled Breaches

6.1.1.1 NRELAP5 Subcooled Modeling Considerations

Subcooled breaches in the primary coolant consist of breaks in the RCS injection and discharge lines and inadvertent operation of the RRV. The model development for the inadvertent RRV opening transient is discussed as follows, since this event is modeled in the dynamic analysis due to its location and size.

Pipe components are used to allow NRELAP5 to determine the time-history changes in the RCS pressure and temperature due to the RRV blowdown event. Five pipes and two branches are used to simulate the different sections of the RCS: the hot leg, cold leg, pressurizer, SG region, core, the lower plenum, and upper plenum in order to implement the temperatures and pressure in the RCS loop. Reactor coolant system volumes and pipe lengths are selected to match the total size of the primary system components. Junctions with no form losses and no choking models are used to connect the pipes. Containment is modeled using a time-dependent volume.

The RCS provides a BC for determining the conditions at the break location. Per Section 5.1.1, it is not necessary to provide a detailed model of the RCS, because the changes in the RCS are small relative to the changes at the break location for the timescales of interest. Dynamic loads can be accurately calculated in ANSYS using BCs from a simplified NRELAP5 model.

The RRV connects directly to the RPV nozzle safe ends.

To simulate the transients, the modeling time step is set at 10 percent of the acoustic Courant limit based on the minimum node length. The time step is increased as the event progresses because the acoustic Courant limit is no longer a consideration once choking occurs; however, the time step is not increased above the material Courant limit. The valve opening time and pipe rupture times are set at 0.001 seconds.

Sensitivity studies are performed for the acoustic Courant limit and variations in the choking model thermal non-equilibrium constant and discharge coefficient. The objective of the sensitivity studies is to qualitatively demonstrate the effect of the modeling parameters on the calculation results, in order to confirm that the parameters recommended via the benchmarking evaluations are appropriate for the design.

Sensitivity studies are performed for the inadvertent RRV opening and the inadvertent RVV opening. These two cases are selected for full sensitivity (i.e., time step, discharging coefficient, thermal non-equilibrium coefficient, and valve opening time) because they are included in dynamic analysis because of their location and size.

Hand calculations are performed to ensure that the thermal hydraulic conditions calculated for the HELBs are reasonable. This is an important step in modeling the NuScale HELBs because some breaks include extrapolation outside of the range of pressures, temperatures, and cross-sectional areas over which HELB methodology benchmarking was performed. This hand calculation provides verification of the accuracy of the simulated results.

The mass flow rate is estimated based on the enthalpy and pressure of the fluid at the break location using Figure 2.20(a) of Reference 7.2.21. The theoretical initial mass flow rate is calculated from the mass flux corresponding to the RCS pressure and enthalpy at the break and the break flow cross-sectional area.

The mass flow rate at the time that the system reaches saturation is also determined. At that time, the system pressure is roughly equal to the initial saturation pressure. The enthalpy can be estimated by assuming the system has come to equilibrium with no change in the system temperature. Note that the energy contribution due to flow is not considered when specifying the stagnation pressure and enthalpy because the assumed pressure and temperature are relevant to the entire RCS, not only the break location.

The Reference 7.2.21 method for estimating the blowdown mass flow rate assumes an isentropic nozzle, and therefore overpredicts the mass flow rate simulated using NRELAP5 with the discharge coefficients recommended in Section 5.1.1. The expected mass flow rate is estimated applying the recommended discharge coefficient reduction.

6.1.1.2 NRELAP5 Subcooled Results

The mass flow rates predicted by NRELAP5 are in good agreement with Figure 2.20(a) of Reference 7.2.21. For the inadvertent RRV opening, there is more than 10 percent variation in mass flow rate from the expected values. However, there is a greater under-prediction for the injection line break at the RPV but this can be attributed to the greater friction and form losses in the RCS injection piping between the riser and the RPV wall. Friction and form losses in the lengths of piping between the RPV nozzle and CNV wall, and a venturi located in the CNV nozzle safe end have an even larger flow-limiting effect for the injection and discharge line breaks at the CNV. Differences may also result in part from errors in estimating the theoretical mass flow rate using Figure 2.20(a) of Reference 7.2.21. In general, Table 6-1 demonstrates that the NRELAP5 results are in good agreement with hand calculations and are appropriate for use. The sensitivity studies demonstrate that the results are reasonable based on the acoustic Courant limit and specified choking model parameters.

Table 6-1 Critical Mass Flow Rate Theoretical, Expected, and NRELAP5 Results

Case	Theoretical Mass Flow Rate (lb/s)	Expected Mass Flow Rate (lb/s)	Peak Mass Flow Rate from NRELAP5 Modeling (lb/s)	Break Location/ Valve Operation
CVCS injection line	{{			Break at RPV
CVCS injection line				Break at CNV
RRV			}}2(a),(c),ECI	RRV opens(1)

Notes:(1) Inadvertent single RRV opening is a design basis event.

The time history pressure, mass flow rate and density results for each break and each set of initial conditions are used to generate the flow acceleration and thrust force ANSYS BCs. Plots of the CVCS injection line pipe break and the RRV opening are provided in Figure 6-1 through Figure 6-4. Figure 6-1 shows fluctuations in the fluid acceleration, which are more pronounced for the RPV terminal end break. These fluctuations are due to small but abrupt changes in the mass flow rate at the break location. The changes in mass flow rate and the calculated fluid acceleration are likely because choked flow conditions have not yet been reached.

Figure 6-1 Flow Acceleration Boundary Condition - Chemical and Volume Control System Injection Pipe Break

{{

}}2(a),(c),ECI

Figure 6-2 Thrust Force Boundary Condition - Chemical and Volume Control System Injection Pipe Break

{{

}}$^{2(a),(c),ECI}$

Figure 6-3 Flow Acceleration Boundary Condition - Reactor Recirculation Valve Inadvertent Opening

{{

}}2(a),(c),ECI

Figure 6-4 Thrust Force Boundary Condition - Reactor Recirculation Valve Inadvertent Opening

{{

}}$^{2(a),(c),ECI}$

6.1.2 NRELAP5 Saturated Breaches

Saturated breaches in the primary coolant consist of breaks in high point degasfication line, operation of the RSV and inadvertent RVV opening.

The model development, sensitivity studies, and analysis process is consistent with Section 6.1.1. The mass flow rates predicted by NRELAP5 are in good agreement with Figure 2.20(a) of Reference 7.2.21. There is an overprediction of mass flow rate for the RVV and RSV operation cases. The higher mass flow rate is attributed to the static quality of the discharge fluid. The theoretical and expected mass flow rates were determined using Figure 2.20(a) of Reference 7.2.21 and assuming a static quality of 1.0; however, the static quality decreases shortly after blowdown as liquid swells in the pressurizer. This results in an increase in the mass flow rate for a given pressure, as shown in Figure 2.20(a). A larger pressurizer level swell results in a higher fluid density at the breach.

In general, Table 6-2 demonstrates that the NRELAP5 results are in good agreement with hand calculations and are appropriate for use in analyses. The sensitivity studies demonstrate the results are reasonable based on the recommended time step and choking model parameters. Plots of the RSV opening and the RVV opening are provided in Figure 6-5 through Figure 6-8 (the high point degasification line result is bounded by the RVV case and therefore, plots for that case are not shown).

Table 6-2 Critical Mass Flow Rate Theoretical, Expected, and NRELAP5 Results

{{

}}2(a),(c),ECI

Figure 6-5 Inadvertent Reactor Safety Valve Opening Flow Acceleration Boundary Condition

{{

}}2(a),(c),ECI

Figure 6-6 Inadvertent Reactor Safety Valve Opening Thrust Force Boundary Condition

{{

}}2(a),(c),ECI

Figure 6-7 Flow Acceleration Boundary Condition- Inadvertent Reactor Vent Valve Opening

{{

}}2(a),(c),ECI

Figure 6-8 Thrust Force Boundary Condition Inadvertent Reactor Vent Valve Opening

{{

}}2(a),(c),ECI

6.2 ANSYS Analysis for Asymmetric Cavity Pressurization and Blowdown

The purpose of the ANSYS analysis is to determine structural loads that result from HELBs in the primary coolant system. Structural loads associated with asymmetric cavity pressurization of the CNV acting simultaneous to the blowdown of the RPV are evaluated. Loads specified in this section contribute to the basis for the mechanical design of the NPM.

Because of the negligible blowdown flow rate resulting from a single SG tube failure, the loads on adjacent RVI are minimal compared to the loads generated due to the design basis pipe breaks, inadvertent RSV opening and inadvertent ECCS valve opening events. As discussed in Section 2.4.1.5, loads due to SG tube rupture are not considered.

The dynamic loads associated with RCS injection line break, reactor safety valve, reactor vent valve, or reactor recirculation valve opening are calculated using transient structural analyses in ANSYS. A single model including two acoustic bodies of CNV and RPV is used to simulate the loads.

Blowdown and asymmetric cavity pressurization loads are not separated because blowdown and asymmetric cavity pressurization are considered to act simultaneously in the dynamic finite element model of the NPM.

In addition to thrust loads acting at the break location, HELBs result in pressure transients associated with propagation of the acoustic wave, acting upon surfaces of the fluid-structure interfaces of the NPM. These pressure transients create dynamic responses of the CNV, RPV, and internal structures, in the horizontal and vertical directions. For each break event, the in-structure acceleration and displacement time history responses are determined at key locations of the CNV, RPV, and internal structures. Also, at key structural cross sections and structural interfaces, the maximum forces and moments due to the most limiting break are provided. The propagation of the pressure wave results in differential pressure loads across internals structures or in transient hoop stresses within axisymmetric structures.

Loads specified in this section apply to the design of the CNV, containment supports, RPV, and reactor internals. Core plate displacement time histories are provided for use in design of the fuel assemblies.

Table 6-3 lists the valve openings and pipe break modeled in the ANSYS modeling cases. Due to the small line size, the pipe breaks are bounded by the loads from some of the valve openings. For example, a RCS discharge line break is bounded by an RVV opening. The RCS injection line break is included in the model. The RCS injection line terminates in the riser, resulting in a pressure wave internal to the riser. A case for each valve opening is presented to portray the impact of valve size and location on asymmetric cavity pressurization loads for nearby components. A case with both RVV1 and RVV2 opening is included.

Table 6-3 Cases for Valve Opening and Break Locations

{{

}}$^{2(a),(c),ECI}$

6.2.1 Geometry

A full geometry model with two acoustic bodies is used for this analysis as shown in Figure 6-9. The minor features do not affect the gross structural behavior of the model and removing them allows for simplified meshing techniques to be used. The mass of existing structures in the model are adjusted to account for these model simplifications. The model mass is compared to the NPM mass calculation and the difference is applied to the model using a combination of point masses, distributed mass elements, and adjusted densities. Additionally, components that are not included in the model, such as the mass of the fuel, are accounted for in the mass of adjacent components. For fuel, the mass is accounted for in the mass specified for the reflector.

Figure 6-9 Full Model with Two Acoustic Bodies

{{

}}$^{2(a),(c),ECI}$

6.2.2 Mesh

The CNV, RPV, lower RVI, upper RVI, RVV, RRV, RSV, and RCS injection line are represented by solid elements. The fluid is represented by acoustic elements. A conformal mesh is created between the fluid and the solid elements to avoid potential convergence issues with dissimilar meshes and contact definitions. An example of this mesh is shown in Figure 6-10. Acoustic elements capture the coupling effect of the FSI at the fluid-structure interface.

Figure 6-10 Meshes for Two Acoustic Bodies

{{

}}$^{2(a),(c),ECI}$

6.2.3 Boundary Conditions

The full blowdown model is supported at the CNV lugs and at the CNV skirt through remote points. The circumferential directions of the remote points for the CNV lugs are constrained and the vertical direction of the CNV skirt bottom surface is constrained. In addition, four nodes at 55 degree, 125 degree, 235 degree, and 305 degree are constrained in the radial direction.

The MS and FW piping connected to the Reactor Building walls are constrained in the lateral directions, the MS and FW piping at wall supports are constrained in three translational degrees of freedom, and the MS and FW piping ends are constrained in the six degrees of freedom.

The acoustic bodies (fluid volumes) and acoustic interfaces (interface between the fluid mesh and the solid mesh) are set using ANSYS parametric design language code.

As discussed in Section 5.1.2, a flow acceleration BC is applied to the acoustic body at the break location along with the thrust force on the solid face. The thrust force is divided by the break area and applied as a pressure.

A time step of 0.0001 seconds is applied for the first 0.01 seconds, a time step of 0.0005 seconds is used up to 0.1 seconds, and a time step of 0.001 is used between 0.1 and 0.2 seconds, to balance the computational time and accuracy. The transient analyses are run for 0.2 seconds.

6.2.4 Time Histories and Maximum Results

The force and moment time histories of the blowdown model are extracted for each of the 8 cases identified in Table 6-3. The absolute maximum force and moment for each time history is calculated. At each location the maximum forces and moments are compared. Only the largest forces and moments are reported.

Maximum forces and moments acting on 123 of the key structural interfaces or supports are listed in Table 6-4. The forces and moments in Table 6-4 are bounding values for the break and valve opening conditions. The component interface locations for the force and momentum generation are listed in Table 6-5.

Table 6-4 Maximum Forces and Moments at Component Interfaces

{{

}}$^{2(a),(c),ECI}$

Table 6-4 Maximum Forces and Moments at Component Interfaces (Continued)

{{

}}2(a),(c),ECI

Table 6-4 Maximum Forces and Moments at Component Interfaces (Continued)

{{

}}2(a),(c),ECI

Table 6-4 Maximum Forces and Moments at Component Interfaces (Continued)

{{

}}2(a),(c),ECI

Table 6-5 List of Component Interfaces for Force and Moment Generation

{{

}}2(a),(c),ECI

Table 6-5 List of Component Interfaces for Force and Moment Generation (Continued)

{{

}}2(a),(c),ECI

Table 6-5 List of Component Interfaces for Force and Moment Generation (Continued)

{{

}}2(a),(c),ECI

Table 6-5 List of Component Interfaces for Force and Moment Generation (Continued)

{{

}}2(a),(c),ECI

Forces and moments are generated for 30 internal sections of NPM components. Time histories are extracted for each node. Maximum forces and moments on the CNV, RPV, riser assemblies, and the core barrel assembly are summarized in Table 6-6. The forces and moments in Table 6-6 are bounding values for the break and valve opening conditions. Locations of the component section for force and momentum are listed in Table 6-7.

Table 6-6 Maximum Forces and Moments Within Component Sections

{{

}}2(a),(c),ECI

Table 6-6 Maximum Forces and Moments Within Component Sections (Continued)

{{

}}$^{2(a),(c),ECI}$

Table 6-7 List of Component Sections for Force and Moment Generation

{{

}}$^{2(a),(c),ECI}$

Table 6-7 List of Component Sections for Force and Moment Generation (Continued)

{{

}}$^{2(a),(c),ECI}$

Table 6-8 identifies the five largest forces acting on RPV, CNV, and RVI in any direction, and Table 6-9 identifies the five largest moments on RPV, CNV, and RVI in any direction. The corresponding event of valve opening associated with each of the forces and moments is identified. The highest forces and moments result from RVV1 and RVV2 opening. The forces on the RPV are one order of magnitude larger than those on the CNV and two orders of magnitude higher than those on the RVI. The largest forces act in the Z direction and generally, the forces in the Z direction are greater than in the X and Y directions at any location for a particular case.

The largest forces generated, by the included scenarios, result from the RVV1 and RVV2 opening and occur within the RPV, from the region just below the feedwater plenum up to just above the PZR heater nozzle.

The RVV1 and RVV2 opening creates the largest moments out of all the cases analyzed. The largest moments act on both the RPV and the CNV, from the region just below steam plenum up to just below pressurizer top and from the CNV flange to CNV ledge for RPV support.

Table 6-8 Summary of Largest Forces for Reactor Pressure Vessel, Containment Vessel, and Reactor Vessel Internals

{{

}}2(a),(c),ECI

Table 6-9 Summary of Largest Moments for Reactor Pressure Vessel, Containment Vessel, and Reactor Vessel Internals

{{

}}2(a),(c),ECI

Table 6-9 Summary of Largest Moments for Reactor Pressure Vessel, Containment Vessel, and Reactor Vessel Internals (Continued)

{{

}}$^{2(a),(c),ECI}$

Table 6-10 and Table 6-11 provide the five largest forces and moments on the RPV, CNV, and RVI due to the CVCS injection line break, including riser locations near where the pressure wave originates. The forces near the riser location for this event are smaller than those experienced for the case of the two RVVs opening per Table 6-8. For the CVCS injection line break event, the forces and moments on many parts of the RPV and CNV are higher than for the reactor vessel internals in magnitude, implying that the pressure wave imparts higher forces on the RPV and CNV structures than RVI. The case of the pressure wave originating from the upper riser assembly is not bounding for mechanical design.

Table 6-10 Five Largest Forces for Chemical and Volume Control System Injection Line Break Event for Reactor Pressure Vessel, Containment Vessel, and Reactor Vessel Internals

{{

}}$^{2(a),(c),ECI}$

Table 6-11 Five Largest Moments for Chemical and Volume Control System Injection Line Break Event for Reactor Pressure Vessel, Containment Vessel, and Reactor Vessel Internals

{{

}}$^{2(a),(c),ECI}$

Figure 6-11 provides a time history plot of the maximum acoustic pressure difference between any point on the top of the baffle plate and any point on the bottom of the baffle plate for the RVV1 opening case. The maximum differential pressure across the baffle plate remains below 9 psi.

Figure 6-11 Differential Pressure Time History Across Pressurizer Baffle Plate

{{

}}2(a),(c),ECI

The differential pressure time histories across the core as the difference between the average pressure at the lower core plate and average pressure at the upper core plate are plotted in Figure 6-12. The maximum differential pressure among all the cases considered is 7.1 psi and occurs for RVV1 and RVV2 opening case.

Figure 6-12 Differential Pressure Time History Across Core

{{

}}2(a),(c),ECI

7.0 References

7.1 Source Documents

7.1.1 American Society of Mechanical Engineers, Quality Assurance Program Requirements for Nuclear Facility Applications, NQA-1-2008, NQA-1a-2009 Addenda, as endorsed by Regulatory Guide 1.28, Rev. 4.

7.1.2 U.S. Code of Federal Regulations, “Quality Assurance Criteria for Nuclear Power Plants and Fuel Reprocessing Facilities,” Appendix B, Part 50, Chapter 1, Title 10, “Energy,” (10 CFR 50).

7.2 Referenced Documents

7.2.1 U.S. Nuclear Regulatory Commission, “Asymmetric Blowdown Loads on PWR Primary Systems, Resolution of Generic Task Action Plan A-2,” NUREG-0609, January 1981.

7.2.2 Watkins, J.C., R5FORCE/MOD3s: A Program to Compute Fluid-Induced Forces Using Hydrodynamic Output from the RELAP5/MOD3 Code, Idaho National Engineering Laboratory, September 1990.

7.2.3 Timperi, A., et al., “Validation of Fluid-Structure Interaction Calculations in a Large Break Loss of Coolant Accident,” ICONE16-48206, 16th International Conference on Nuclear Engineering, Orlando, FL, May 2008.

7.2.4 Kähkönen, J., P. Varpasuo, M. Vuorinen, “Analyzing HDR Fluid-Structure-Interaction Pipe Break Case with Acoustic Finite Element Method,” ICONE19-43205, 19th International Conference on Nuclear Engineering, Chiba, Japan, May 2011.

7.2.5 Wolf, L., “Experimental Results of Coupled Fluid-Structure Interactions during Blowdown of the HDR-vessel and Comparisons with Pre- and Post-test Predictions,” Nuclear Engineering and Design, Vol. 70, 269-308, 1982.

7.2.6 Prelewicz, D.A., “Hydraulic Pressure Pulses with Structural Flexibility: Test and Analysis, WAPD-TM-1227,” Bettis Atomic Power Laboratory, West Mifflin, PA, April 1976.

7.2.7 Mitsubishi Heavy Industries, Ltd, “Subcompartment Analyses for US-APWR Design Confirmation,” US-APWR, MUAP-07031-NP, Rev. 1, Nonproprietary, October 2009.

7.2.8 Brandt, T., et al., “Validation of fluid-structure interaction simulation environment in analysis of large-break loss of coolant accident,” System Simulation and Scientific Computing, pp. 520-527, October 2008.

7.2.9 Allemann, R.T., et al., Battelle Pacific Northwest Laboratories, "AEC Research and Development Report: Coolant Blowdown Studies of a Reactor Simulator Vessel containing a Simulated Reactor Core," BNWL-1524, June 1971.

7.2.10 Christensen, D.D., EG&G Idaho, Inc., "United States Standard Problem 5, Final Report," PG-R-77-44, December 1977.

7.2.11 Delaney, H.M., EG&G Idaho, Inc., "United States Standard Problem 6 and International Standard Problem 4, Final Report," CVAP-TR-4-78, March 1978.

7.2.12 Brockett, G.F., et al., EG&G Idaho, Inc., "Experimental Investigations of Reactor System Blowdown," IN-1348, September 1970.

7.2.13 Robinson, H.C., EG&G Idaho, Inc., "Experimental Data Report for LOFT Nonnuclear Test LI-2," TREE-NUREG-1026, January 1977.

7.2.14 Fritz, R.J., and E. Kiss, General Electric Company, "The Vibration Response of a Cantilevered Cylinder Surrounded by an Annular Fluid," KAPL-M-6539 (RJF-10), February 24, 1966.

7.2.15 Prelewicz, D.A., "Hydraulic Pressure Pulses with Structural Flexibility: Test and Analysis," WAPD-TM-1227, Bettis Atomic Power Laboratory, West Mifflin, PA, April 1976.

7.2.16 Electric Power Research Institute, "Comparison of the Calculation of HDR RPV-1 Blowdown Loads for Test V32 with the Experimental Data," NP-3677, EPRI, Palo Alto, CA, August 1984.

7.2.17 INEEL-EXT-98-00834-V5, RELAP5-3D© Code Manual Volume V: User's Guidelines, Rev. 4.1, September 2013.

7.2.18 Rosdahl, O., and D. Caraher, U.S. Nuclear Regulatory Commission, "Assessment of RELAP5/MOD 2 Against Critical Flow Data From Marviken Tests JIT 11 and CFT 21." NUREG/IA-0007, September 1986.

7.2.19 INEEL-EXT-98-00834-V4, RELAP5-3D© Code Manual Volume IV: Models and Correlations, Rev. 4.1, September 2013.

7.2.20 Schumann, U., Experimental and Computed Results for Fluid-Structure Interactions with Impacts in the HDR Blowdown Experiment, Nuclear Engineering and Design 73 (1982): 303-317.

7.2.21 Moody, F. J., Introduction to Unsteady Thermofluid Mechanics, John Wiley & Sons, New York, NY, 1990.

7.2.22 Electric Power Research Institute, "Two-Phase Jet Modeling and Data Comparison," NP-4362, EPRI, Palo Alto, CA, March 1986.

7.2.23 Wolf, L., “Design Report for the HDR-RPV-I Blowdown Experiments V31.2, V32, V33, and V34 with Specifications for the Pretest Computation,” HDR Safety Program, Report No. 3.243/81, Battelle Institute, Frankfurt, 1981.

7.2.24 ANSYS® Mechanical, Release 2019 R1, ANSYS, Inc., Canonsburg, PA 2019.

Appendix A NRELAP5 Heissdampf Reactor and Jet Impingement Test Results

Figure A-1 Heissdampf Reactor Test V31.1 Sensitivity Case A2, Mass Flow Rate

{{

}}2(a),(c),ECI

Figure A-2 Heissdampf Reactor Test V31.1 Sensitivity Case A2, Pressure

{{

}}$^{2(a),(c),ECI}$

Figure A-3 Heissdampf Reactor Test V31.1 Sensitivity Case A5, Mass Flow Rate

{{

}}2(a),(c),ECI

Figure A-4 Heissdampf Reactor Test V31.1 Sensitivity Case A5, Pressure

{{

}}2(a),(c),ECI

Figure A-5 Heissdampf Reactor Test V31.1 Sensitivity Case A8, Mass Flow Rate

{{

}}$^{2(a),(c),ECI}$

Figure A-6 Heissdampf Reactor Test V31.1 Sensitivity Case A8

{{

}}$^{2(a),(c),ECI}$

Figure A-7 Heissdampf Reactor Test V31.1 Sensitivity Case B, Pressure

{{

}}2(a),(c),ECI

Figure A-8 Heissdampf Reactor Test V31.1 Sensitivity Case B2, Pressure

{{

}}$^{2(a),(c),ECI}$

Figure A-9 Heissdampf Reactor Test V31.1 Sensitivity Case Set B, Mass Flow Rate

{{

}}$^{2(a),(c),ECI}$

Figure A-10 Heissdampf Reactor Test V31.1 Sensitivity Case B2, Mass Flow Rate

{{

}}2(a),(c),ECI

Figure A-11 Heissdampf Reactor Test V31.1 Sensitivity Case Set C, Mass Flow Rate

{{

}}$^{2(a),(c),ECI}$

Figure A-12 Heissdampf Reactor Test V31.1 Sensitivity Case Set C, Pressure

{{

}}$^{2(a),(c),ECI}$

Figure A-13 Mass Flow Rate for Heissdampf Reactor Test V31.1

{{

}}$^{2(a),(c),ECI}$

Figure A-14 Mass Flow Rate for Heissdampf Reactor Test V32

{{

}}$^{2(a),(c),ECI}$

Figure A-15 Mass Flow Rate for Marviken Jet Impingement Test-11

{{

}}2(a),(c),ECI

Figure A-16 Density for Marviken Jet Impingement Test-11

{{

}}$^{2(a),(c),ECI}$

Figure A-17 Thrust Force for Marviken Jet Impingement Test-11

{{

}}$^{2(a),(c),ECI}$

Appendix B Pressure Comparison for Bettis Hydraulic Pressure Pulse

Figure B-1 Pressure at Top and Bottom Transducers for Run 10S

{{

}}$^{2(a),(c),ECI}$

Figure B-2 Pressure at Top and Bottom Transducers for Run 10F

{{

}}2(a),(c),ECI

Figure B-3 Pressure at Top and Bottom Transducers for Run 20S

{{

}}$^{2(a),(c),ECI}$

Figure B-4 Pressure at Top and Bottom Transducers for Run 20F

{{

}}2(a),(c),ECI

Appendix C Thrust Force and Fluid Acceleration Boundary Conditions

Figure C-1 Flow Acceleration at the Break Location for Heissdampf Reactor Test V29.2

{{

}}$^{2(a),(c),ECI}$

Figure C-2 Thrust Force at the Break Location for Heissdampf Reactor Test V29.2

{{

}}2(a),(c),ECI

Figure C-3 Flow Acceleration at the Break Location for Heissdampf Reactor Test V31.1

{{

}}2(a),(c),ECI

Figure C-4 Thrust Force at the Break Location for Heissdampf Reactor Test V31.1

{{

}}$^{2(a),(c),ECI}$

Figure C-5 Flow Acceleration at the Break Location for Heissdampf Reactor Test V32

{{

}}$^{2(a),(c),ECI}$

Figure C-6 Thrust Rorce at the Break Location for Heissdampf Reactor Test V32

{{

}}2(a),(c),ECI

Appendix D ANSYS Heissdampf Reactor Results with Pressure Boundary Condition

Figure D-1 Heissdampf Reactor Test V31.1 Pressure, BP9109 (1330, 90°, 8850) (Fig. 4-5 of Reference 7.2.16)

{{

}}$^{2(a),(c),ECI}$

Figure D-2 Heissdampf Reactor Test V31.1 Pressure, KP0009 (1307, 90°, 8850) (Fig. 4-12 of Reference 7.2.16)

{{

}}$^{2(a),(c),ECI}$

Figure D-3 Displacement Comparison for Heissdampf Reactor Test V32, KS1030 (1307, 90°, 2265) (Fig. A-118 of Reference 7.2.16)

{{

}}$^{2(a),(c),ECI}$

Figure D-4 Displacement Comparison for Heissdampf Reactor Test V32, KS1032 (1307, 270°, 2265) (Fig. A-120 of Reference 7.2.16)

{{

}}2(a),(c),ECI

Appendix E Heissdampf Reactor V29.2 ANSYS Results, Mass Flow Rate Boundary Condition

Figure E-1 Displacement at Upper Part of the Core Barrel for V29.2, KS1008 (1330, 90°, 8410) (Fig. 26 of Reference 7.2.5)

{{

}}$^{2(a),(c),ECI}$

Figure E-2 Outside Reactor Pressure Vessel Displacement for V29.2, BS0106 (1590, 90°, 7350) (Fig. 28 of Reference 7.2.5)

{{

}}2(a),(c),ECI

Figure E-3 Outside Reactor Pressure Vessel Displacement for V29.2, BS0107 (1590, 180°, 7350) (Fig. 28 of Reference 7.2.5)

{{

}}2(a),(c),ECI

Figure E-4 Outside Reactor Pressure Vessel Displacement for V29.2, BS0108 (1590, 270°, 7350) (Fig. 28 of Reference 7.2.5)

{{

}}$^{2(a),(c),ECI}$

Appendix F Heissdampf Reactor V31.1 ANSYS Results, Mass Flow Rate Boundary Condition

Figure F-1 Outside Reactor Pressure Vessel for V31.1, BS0106 (1590, 90°, 7350) (Fig. 28 of Reference 7.2.5)

{{

}}$^{2(a),(c),ECI}$

Figure F-2 Outside Reactor Pressure Vessel for V31.1, BS0107 (1590, 180°, 7350) (Fig. 28 of Reference 7.2.5)

{{

}}$^{2(a),(c),ECI}$

Figure F-3 Outside Reactor Pressure Vessel Displacement for V31.1, BS0108 (1590, 270°, 7350) (Fig. 28 of Reference 7.2.5)

{{

}}$^{2(a),(c),ECI}$

Figure F-4 Pressure for V31.1, BP9109 (1330, 90°, 8850) (Fig. 4-5 of Reference 7.2.16)

{{

}}$^{2(a),(c),ECI}$

Figure F-5 Pressure for V31.1, BP9117 (1330, 270°, 8850) (Fig. 4-6 of Reference 7.2.16)

{{

}}$^{2(a),(c),ECI}$

Figure F-6 Pressure for V31.1, BP9133 (1330, 88°, 5505) (Fig. 4-7 of Reference 7.2.16)

{{

}}$^{2(a),(c),ECI}$

Figure F-7 Pressure for V31.1, BP9140 (1330, 90°, 2300) (Fig. 4-8 of Reference 7.2.16)

{{

}}$^{2(a),(c),ECI}$

Figure F-8 Pressure for V31.1, BP8301 (0, 0°, 10370) (Fig. 4-10 of Reference 7.2.16)

{{

}}2(a),(c),ECI

Figure F-9 Differential Pressure for V31.1, KP0009 (1307, 90°, 8850) (Fig. 4-12 of Reference 7.2.16)

{{

}}2(a),(c),ECI

Figure F-10 Hoop Strain for V31.1, at Core Barrel Outside Diameter KA2009 (1330, 90°, 8850) (Fig. 4-15 of Reference 7.2.16)

{{

}}$^{2(a),(c),ECI}$

Figure F-11 Axial Strain for V31.1, at Core Barrel Outside Diameter KA3008 (1330, 90°, 8850) (Fig. 4-16 of Reference 7.2.16)

{{

}}2(a),(c),ECI

Appendix G Heissdampf Reactor V32 ANSYS Results, Mass Flow Rate Boundary Condition

Figure G-1 Outside Reactor Pressure Vessel Displacement for V32, BS0106 (1590, 90°, 7350) (Fig. 8 of Reference 7.2.20)

{{

}}2(a),(c),ECI

Figure G-2 Outside Reactor Pressure Vessel Displacement for V32, BS0116 (1590, 90°, 5550) (Fig. A-47 of Reference 7.2.16)

{{

}}2(a),(c),ECI

Figure G-3 Core Barrel Displacement for V32, KS1013 (1307, 90°, 7195) (Fig. A-112 of Reference 7.2.16)

{{

}}2(a),(c),ECI

Figure G-4 Core Barrel Displacement for V32, KS1030 (1307, 90°, 2265) (Fig. A-118 of Reference 7.2.16)

{{

}}$^{2(a),(c),ECI}$

Figure G-5 Core Barrel Displacement for V32, KS1032 (1307, 270°, 2265) (Fig. A-120 of Reference 7.2.16)

{{

}}2(a),(c),ECI

Figure G-6 Core Barrel Hoop Strain for V32, KA2008 (1330, 90°, 8845) (Fig. A-66 of Reference 7.2.16)

{{

}}2(a),(c),ECI

Figure G-7 Core Barrel Axial Strain for V32, KA3009 (1330, 90°, 8825) (Fig. A-71 of Reference 7.2.16)

{{

}}2(a),(c),ECI

Figure G-8 Sensitivity Study: Core Barrel Displacement for V32, KA1030 (1307, 90°, 2265) (Fig. A-118 of Reference 7.2.16)

{{

}}$^{2(a),(c),ECI}$

Figure G-9 Sensitivity Study: Core Barrel Displacement for V32, KA1032 (1307, 270°, 2265) (Fig. A-120 of Reference 7.2.16)

{{

}}$^{2(a),(c),ECI}$

Figure G-10 Sensitivity Study: Core Barrel Hoop Strain for V32, KA2008 (1330, 90°, 8845) (Fig. A-66 of Reference 7.2.16)

{{

}}$^{2(a),(c),ECI}$

Figure G-11 Sensitivity Study: Core Barrel Axial Strain for V32, KA3009 (1330, 90°, 8825) (Fig. A-71 of Reference 7.2.16)

{{

}}$^{2(a),(c),ECI}$

Enclosure 3:

Affidavit of Carrie Fosaaen, AF-173482

NuScale Power, LLC

AFFIDAVIT of Carrie Fosaaen

I, Carrie Fosaaen, state as follows:

(1) I am the Vice President of Regulatory Affairs of NuScale Power, LLC (NuScale), and as such, I have been specifically delegated the function of reviewing the information described in this Affidavit that NuScale seeks to have withheld from public disclosure, and am authorized to apply for its withholding on behalf of NuScale

(2) I am knowledgeable of the criteria and procedures used by NuScale in designating information as a trade secret, privileged, or as confidential commercial or financial information. This request to withhold information from public disclosure is driven by one or more of the following:

(a) The information requested to be withheld reveals distinguishing aspects of a process (or component, structure, tool, method, etc.) whose use by NuScale competitors, without a license from NuScale, would constitute a competitive economic disadvantage to NuScale.

(b) The information requested to be withheld consists of supporting data, including test data, relative to a process (or component, structure, tool, method, etc.), and the application of the data secures a competitive economic advantage, as described more fully in paragraph 3 of this Affidavit.

(c) Use by a competitor of the information requested to be withheld would reduce the competitor's expenditure of resources, or improve its competitive position, in the design, manufacture, shipment, installation, assurance of quality, or licensing of a similar product.

(d) The information requested to be withheld reveals cost or price information, production capabilities, budget levels, or commercial strategies of NuScale.

(e) The information requested to be withheld consists of patentable ideas.

(3) Public disclosure of the information sought to be withheld is likely to cause substantial harm to NuScale's competitive position and foreclose or reduce the availability of profit-making opportunities. The accompanying report reveals distinguishing aspects about the process by which NuScale develops its Module Short-Term Transient Analysis.

NuScale has performed significant research and evaluation to develop a basis for this process and has invested significant resources, including the expenditure of a considerable sum of money.

The precise financial value of the information is difficult to quantify, but it is a key element of the design basis for a NuScale plant and, therefore, has substantial value to NuScale.

If the information were disclosed to the public, NuScale's competitors would have access to the information without purchasing the right to use it or having been required to undertake a similar expenditure of resources. Such disclosure would constitute a misappropriation of NuScale's intellectual property, and would deprive NuScale of the opportunity to exercise its competitive advantage to seek an adequate return on its investment.

(4) The information sought to be withheld is in the enclosed report entitled, NuScale Power, LLC Submittal of NuScale Power Module Short-Term Transient Analysis, TR-121517-P, Revision 1. The enclosure contains the designation "Proprietary" at the top of each page containing proprietary information. The information considered by NuScale to be proprietary is identified within double braces, "{{ }}" in the document.

(5) The basis for proposing that the information be withheld is that NuScale treats the information as a trade secret, privileged, or as confidential commercial or financial information. NuScale relies upon the exemption from disclosure set forth in the Freedom of Information Act ("FOIA"), 5 USC § 552(b)(4), as well as exemptions applicable to the NRC under 10 CFR §§ 2.390(a)(4) and 9.17(a)(4).

(6) Pursuant to the provisions set forth in 10 CFR § 2.390(b)(4), the following is provided for consideration by the Commission in determining whether the information sought to be withheld from public disclosure should be withheld:

(a) The information sought to be withheld is owned and has been held in confidence by NuScale.

(b) The information is of a sort customarily held in confidence by NuScale and, to the best of my knowledge and belief, consistently has been held in confidence by NuScale. The procedure for approval of external release of such information typically requires review by the staff manager, project manager, chief technology officer or other equivalent authority, or the manager of the cognizant marketing function (or his delegate), for technical content, competitive effect, and determination of the accuracy of the proprietary designation. Disclosures outside NuScale are limited to regulatory bodies, customers and potential customers and their agents, suppliers, licensees, and others with a legitimate need for the information, and then only in accordance with appropriate regulatory provisions or contractual agreements to maintain confidentiality.

(c) The information is being transmitted to and received by the NRC in confidence.

(d) No public disclosure of the information has been made, and it is not available in public sources. All disclosures to third parties, including any required transmittals to NRC, have been made, or must be made, pursuant to regulatory provisions or contractual agreements that provide for maintenance of the information in confidence.

(e) Public disclosure of the information is likely to cause substantial harm to the competitive position of NuScale, taking into account the value of the information to NuScale, the amount of effort and money expended by NuScale in developing the information, and the difficulty others would have in acquiring or duplicating the information. The information sought to be withheld is part of NuScale's technology that provides NuScale with a competitive advantage over other firms in the industry. NuScale has invested significant human and financial capital in developing this technology and NuScale believes it would be difficult for others to duplicate the technology without access to the information sought to be withheld.

I declare under penalty of perjury that the foregoing is true and correct. Executed on August 30, 2024.

Carrie Fosaaen